

---

# Feature-aligned N-BEATS with Sinkhorn divergence

---

Myeongho Jeon<sup>\*,1</sup> Myungjoo Kang<sup>†,1</sup> Joonhun Lee<sup>\*,1</sup> Kyunghyun Park<sup>†,2</sup>

<sup>1</sup>Seoul National University

<sup>2</sup>Nanyang Technological University

## Abstract

In this study, we propose Feature-aligned N-BEATS as a domain generalization model for univariate time series forecasting problems. The proposed model is an extension of the doubly residual stacking architecture of N-BEATS (Oreshkin et al. [34]) into a representation learning framework. The model is a new structure that involves marginal feature probability measures (i.e., pushforward measures of multiple source domains) induced by the intricate composition of residual operators of N-BEATS in each stack and aligns them stack-wise via an entropic regularized Wasserstein distance referred to as the Sinkhorn divergence (Genevay et al. [14]). The loss function consists of a typical forecasting loss for multiple source domains and an alignment loss calculated with the Sinkhorn divergence, which allows the model to learn invariant features stack-wise across multiple source data sequences while retaining N-BEATS’s interpretable design. We conduct a comprehensive experimental evaluation of the proposed approach and the results demonstrate the model’s forecasting and generalization capabilities in comparison with methods based on the original N-BEATS.

## 1 Introduction

Machine learning models are typically proposed under the premise that the minimization of loss on a training distribution results in enhanced performance on a testing distribution, i.e., empirical risk minimization [42]. However, when deploying those models to real-world scenarios, an unknown target distribution often deviates substantially from the training distribution, posing challenges for effective model adaptation. This predicament is closely linked to the concept of domain shift in the machine learning literature [38].

In response to this, a multitude of studies has expanded the domain generalization (or adaptation) research [45, 46, 44]. In particular, classification tasks have been the predominant focus within these research areas [12, 22, 24]. Although several studies have discussed domain shift in the context of time series forecasting [19, 35, 20], this direction has not received substantial emphasis contrary to classification tasks. On the other hand, a recent deep neural network model employing doubly residual stacking principle (N-BEATS) [34] demonstrates remarkable forecasting capabilities and notable generalizability for time series data [35].

From these observations, we aim to propose Feature-aligned N-BEATS, a domain generalization model extending the doubly residual stacking architecture for univariate time series forecasting. To achieve this, we incorporate a specialized toolkit for learning invariant features within the doubly residual stacking architecture. In representation learning theory [5], the alignment (or regularization) of marginal feature measures (or distributions) is commonly employed for learning feature invariance. Many studies [31, 22, 28, 52] demonstrated that feature alignment is an effective resolution to domain

---

\*Equal contribution (andyjeon@snu.ac.kr, nicegyu718@snu.ac.kr)

†Co-corresponding authors (mkang@snu.ac.kr, kyunghyun.park@ntu.edu.sg)

generalization capabilities for classification tasks. On the other hand, the presence of multiple feature extractors within the doubly residual stacking architecture makes it challenging to define feature alignment in the backbone structure. Moreover, by the nature of time series forecasting, scale and dimensionality issues arise when dealing with both extremely distinct source domains and long-term forecasting tasks.

To resolve these challenges, we devise a stack-wise alignment approach that aligns feature measures induced by the composition of residual operators and a normalization operator. This alignment process involves minimizing divergences between the feature measures on a stack-wise basis. This enables the model to learn invariant features for each stack while preserving the interpretability of the original N-BEATS (Section 4.1). In our approach, we utilize the Sinkhorn divergence [14] for the distance metric for stack-wise alignment. The inspiration for this choice comes from the adversarial framework [16], where an optimal transport distance is employed to calculate the divergence between a pushforward measure (induced by a generator) and a target measure. The Sinkhorn divergence, being an entropic regularized OT distance, has been recently employed in an adversarial framework for generating time series data [49]. Given that our feature measures are defined as pushforward measures and our objective is time series forecasting, we adopt the Sinkhorn divergence as the distance metric (Section 4.2). The training objective in our model is essentially the minimization of forecasting loss across multiple source domains, combined with the stack-wise Sinkhorn divergence between marginal feature measures (Section 4.3).

Furthermore, we provide detailed descriptions of N-BEATS architecture along with its associated properties (Lemma 4.1). From this, we derive a representation learning bound (Theorem 4.1) based on the entropic regularized Wasserstein distance, which supports the feasibility of the stack-wise alignment. In Section 5, we provide a comprehensive evaluation analysis with real-world data, which demonstrates the generalization and forecasting capabilities of Feature-aligned N-BEATS.

## 2 Related Work

Recurrent neural networks have emerged as a prominent architectural choice for sequence prediction tasks, and their utilization in forecasting has been considerably widespread [6, 39, 40, 4, 18]. Convolutional neural networks are utilized in time series forecasting for their capacity to extract local features and capture patterns invariant to their position within the sequence [8, 26]. Transformer-based methodologies employ self-attention mechanisms to capture temporal dependencies [25, 53, 48, 54, 47, 27, 50]. However, [50] argued that the permutation-invariant self-attention mechanism inherent in transformers leads to the loss of temporal information and demonstrates through experiments that a simple linear model outperforms sophisticated transformers in terms of performance. In contrast, multilayer perceptron-based approaches are devoid of these constraints, surpassing state-of-the-art transformer models in their empirical analyses [34, 7].

Recent advancements have introduced approaches to address robustness in domain shifts for time series data. [19] proposed sampling source domains resembling the target domain and employing regularization to encourage domain-invariant representations. [20] introduced a shared attention module with a domain discriminator to achieve domain-invariant features, while private modules capture domain-specific features. Additionally, [35] integrated domain generalization into time series forecasting, addressing situations with unknown target distributions during training within the framework of meta-learning. Nonetheless, an explicit toolkit for domain generalization is not considered in [35].

## 3 Background

**Notation.** We define the input and output spaces as  $\mathcal{X} := \mathbb{R}^\alpha$  and  $\mathcal{Y} := \mathbb{R}^\beta$ , where  $\alpha$  and  $\beta$  represent the lookback and forecast horizons, respectively. The latent space is denoted as  $\mathcal{Z} := \mathbb{R}^\gamma$ , with  $\gamma$  representing the feature dimension. We also consider a subspace of the latent space as  $\tilde{\mathcal{Z}} \subset \mathcal{Z}$ . All the aforementioned spaces are equipped with the Euclidean norm  $\|\cdot\|$ .

We define  $\mathcal{P} := \mathcal{P}(\mathcal{X} \times \mathcal{Y})$  as the set of all Borel joint probability measures on  $\mathcal{X} \times \mathcal{Y}$ . For any  $\mathbb{P} \in \mathcal{P}$ ,  $\mathbb{P}_{\mathcal{X}}$  and  $\mathbb{P}_{\mathcal{Y}}$  represent its marginal probability measures on  $\mathcal{X}$  and  $\mathcal{Y}$ , respectively. Furthermore,  $\mathcal{P}(\mathcal{X})$  and  $\mathcal{P}(\tilde{\mathcal{Z}})$  denote the sets of all Borel probability measures on  $\mathcal{X}$  and  $\tilde{\mathcal{Z}}$ , respectively.

### 3.1 Domain generalization in time series forecasting

We consider a domain generalization task for univariate time series forecasting, in which there exists multiple source (or observable) domains  $\{\mathcal{D}^k\}_{k=1}^K$  with  $K \geq 2$  and target (or unseen) domain  $\mathcal{D}^T$ . Each source domain  $\mathcal{D}^k$  is associated with a probability measure  $\mathbb{P}^k \in \mathcal{P}$  and the same holds for the target domain  $\mathcal{D}^T$  with  $\mathbb{P}^T \in \mathcal{P}$ . The time series sequences within each domain are sampled from their respective joint distributions. Then, the objective is to derive a prediction model  $\mathfrak{F} : \mathcal{X} \rightarrow \mathcal{Y}$  such that  $\mathfrak{F}(\mathbf{s}_{t-\alpha+1}, \dots, \mathbf{s}_t) \approx \mathbf{s}_{t+1}, \dots, \mathbf{s}_{t+\beta}$  for any  $\mathbf{s} = (\mathbf{s}_{t-\alpha+1}, \dots, \mathbf{s}_t) \times (\mathbf{s}_{t+1}, \dots, \mathbf{s}_{t+\beta}) \sim \mathbb{P}^T$ , by leveraging on  $\{\mathbb{P}^k\}_{k=1}^K$ , i.e.,

$$\inf_{\mathfrak{F}} \mathcal{L}(\mathfrak{F}), \quad \text{with} \quad \mathcal{L}(\mathfrak{F}) := \frac{1}{K} \sum_{k=1}^K \mathbb{E}_{(x,y) \sim \mathbb{P}^k} [l(\mathfrak{F}(x), y)], \quad (1)$$

and  $l : \mathcal{Y} \times \mathcal{Y} \rightarrow \mathbb{R}_+$  denoting a loss function.

This task involves a fundamental challenge of learning common features across diverse domains' sequences in addition to achieving accurate forecasting performance for an unknown target domain.

### 3.2 Doubly residual stacking architecture

The essential structure of doubly residual architectures in [34, 7] is summarized as follows: Given  $M, L \in \mathbb{N}$ , the model comprises  $M$  stacks, with each stack consisting of  $L$  blocks. These blocks share the same model weight within their respective stack and are recurrently operated using the double residual stacking principle. More precisely, an  $m$ -th stack derives the doubly residual principle in a way that for any  $m = 1, \dots, M$  and  $x_{m,1} \in \mathcal{X}$ ,

$$\hat{y}_m := \sum_{l=1}^L (\xi_{\downarrow}^m \circ \psi^m)(x_{m,l}), \quad x_{m,l} := x_{m,l-1} - (\xi_{\uparrow}^m \circ \psi^m)(x_{m,l-1}), \quad l = 2, \dots, L, \quad (2)$$

where  $\psi^m : \mathcal{X} \rightarrow \mathcal{Z}$  extracts features  $\psi^m(x_{m,l}) \in \mathcal{Z}$  from the inputs  $x_{m,l} \in \mathcal{X}$  for each layer  $l$ , and then  $(\xi_{\downarrow}^m, \xi_{\uparrow}^m) : \mathcal{Z} \rightarrow \mathcal{Y} \times \mathcal{X}$  generates both forecasts  $(\xi_{\downarrow}^m \circ \psi^m)(x_{m,l}) \in \mathcal{Y}$  and backcasts  $(\xi_{\uparrow}^m \circ \psi^m)(x_{m,l}) \in \mathcal{X}$  branches of sequences. Note that  $\hat{y}_m \in \mathcal{Y}$  represents a stack forecast obtained through the hierarchical aggregation of each block's forecast. Additionally, the last backcast  $x_{m,L} \in \mathcal{X}$ , derived by a residual sequence from blocks, serves as an input for the next stack, except when  $m = M$ .

Once the hierarchical aggregation of all stacks and the residual operations are completed, a prediction model  $\mathfrak{F}$  for the doubly residual stacking architecture is given by the following equations: for any  $(x, y) \sim \mathbb{P}^T$  with  $x_{1,1} := x$ ,

$$y \approx \mathfrak{F}(x; \Psi, \Xi_{\downarrow}, \Xi_{\uparrow}) := \sum_{m=1}^M \hat{y}_m, \quad x_{m,1} := x_{m-1,L}, \quad m = 2, \dots, M, \quad (3)$$

subject to  $\hat{y}_m$  and  $x_{m-1,L}$  in (2), where  $\Psi := \{\psi^m\}_{m=1}^M$ ,  $\Xi_{\downarrow} := \{\xi_{\downarrow}^m\}_{m=1}^M$ , and  $\Xi_{\uparrow} := \{\xi_{\uparrow}^m\}_{m=1}^M$  are implemented by pure deep learning architecture consisting of fully-connected layers (for detailed configuration, please refer to Appendix A. of Supplementary Material).

### 3.3 Domain-invariant feature representation

Learning domain-invariant feature representations has been an effective approach to enhance domain generalization capabilities in classification tasks [31, 22, 28, 52]. In particular, [52] introduced a regularization term based on the adversarial learning framework [16], which enables their image classification model to learn invariant features across diverse source domains. Building upon the error analysis in domain adaptation models in [51], [1] proposed a new analysis on domain generalization models for classification tasks. This provides us valuable insight for developing a domain generalization toolkit within the context of doubly residual stacking models.

The following proposition restates the analysis in [1, Theorem 1]. Before that, we introduce some notation for their classification tasks. Denote by  $\mathcal{H}$  a class of hypothesis functions  $h : \mathcal{X} \rightarrow [0, 1]$  and by  $d_{\mathcal{H}}(\mathbb{P}'_{\mathcal{X}}, \mathbb{P}''_{\mathcal{X}}) := 2 \sup_{h \in \mathcal{H}} |\mathbb{E}_{x \sim \mathbb{P}'_{\mathcal{X}}} [\mathbf{1}_{\{h(x)=1\}}] - \mathbb{E}_{x \sim \mathbb{P}''_{\mathcal{X}}} [\mathbf{1}_{\{h(x)=1\}}]|$  an  $\mathcal{H}$ -divergence between

any measures  $\mathbb{P}'_{\mathcal{X}}, \mathbb{P}''_{\mathcal{X}} \in \mathcal{P}(\mathcal{X})$ . For the class  $\mathcal{H}$ , further denote by  $\tilde{\mathcal{H}} := \{\text{sgn}(|h(\cdot) - h'(\cdot)| - t) : \forall h, h' \in \mathcal{H}, t \in [0, 1]\}$ , which induces marginal feature measures (see [51, Section 4.2], [1, Section 3.3]), and by  $d_{\tilde{\mathcal{H}}}(\cdot, \cdot)$  the corresponding  $\tilde{\mathcal{H}}$ -divergence on  $\mathcal{P}(\mathcal{X})$ .

**Proposition 3.1** ([1, Theorem 1]). *Consider a convex hull of  $\{\mathbb{P}_{\mathcal{X}}^k\}_{k=1}^K$ , i.e.,  $\Lambda := \{\sum_{k=1}^K \pi_k \mathbb{P}_{\mathcal{X}}^k \mid \pi \in \Delta_K\}$ , where  $\Delta_K$  is a  $(K-1)$ -dimensional simplex such that each  $\pi$  represents a convex weight. Denote by  $\mathbb{P}^* := \sum_{k=1}^K \pi_k^* \mathbb{P}_{\mathcal{X}}^k \in \Lambda$  a minimizer such that  $d_{\mathcal{H}}(\mathbb{P}_{\mathcal{X}}^T, \mathbb{P}_{\mathcal{X}}^*) = \min_{\mathbb{P}'_{\mathcal{X}} \in \Lambda} d_{\mathcal{H}}(\mathbb{P}_{\mathcal{X}}^T, \mathbb{P}'_{\mathcal{X}})$ . Then an expected risk  $\epsilon^T$  under target measure  $\mathbb{P}_{\mathcal{X}}^T$  has an upper bound given as*

$$\epsilon^T(h) \leq \sum_{k=1}^K \pi_k^* \epsilon^k(h) + d_{\mathcal{H}}(\mathbb{P}_{\mathcal{X}}^T, \mathbb{P}_{\mathcal{X}}^*) + \max_{i,j \in \{1, \dots, K\}, i \neq j} d_{\tilde{\mathcal{H}}}(\mathbb{P}_{\mathcal{X}}^i, \mathbb{P}_{\mathcal{X}}^j) + \lambda_{(\mathbb{P}_{\mathcal{X}}^T, \mathbb{P}_{\mathcal{X}}^*)}, \quad \forall h \in \mathcal{H}, \quad (4)$$

where  $\lambda_{(\mathbb{P}_{\mathcal{X}}^T, \mathbb{P}_{\mathcal{X}}^*)} := \min\{\mathbb{E}_{x \sim \mathbb{P}_{\mathcal{X}}^T} [|f^*(x) - f^T(x)|], \mathbb{E}_{x \sim \mathbb{P}_{\mathcal{X}}^*} [|f^*(x) - f^T(x)|]\}$  with  $f^* := \sum_{k=1}^K \pi_k^* f^k$ , and each  $f^k$  denotes a true labeling function under  $\mathbb{P}^k$  (i.e.,  $y = f^k(x) \forall (x, y) \sim \mathbb{P}^k$ ), and similarly  $f^T$  denotes a true labeling function under  $\mathbb{P}^T$ .

While the upper bound in (4) comprises four terms depending on distributional relation between the target domain and the multiple source domains, the first and third terms (representing the source risks, i.e.,  $\{\epsilon^k\}_{k=1}^K$  and the pairwise divergences across all marginal feature measures, i.e.,  $\{d_{\tilde{\mathcal{H}}}(\mathbb{P}_{\mathcal{X}}^i, \mathbb{P}_{\mathcal{X}}^j)\}_{i \neq j}^K$ , respectively) are what models can learn within source domains. Inspired by this theoretical evidence and the representation learning framework, we propose a domain generalization model for time series forecasting problems by building on the doubly residual stacking architecture with a feature-alignment toolkit embracing the divergence of marginal feature measures.

## 4 Method

### 4.1 Stack-wise marginal feature measures.

Aligning marginal feature measures is the predominant approach in domain-invariant representation learning [12, 41]. These measures, referred to as pushforward measures  $\{g_{\#} \mathbb{P}_{\mathcal{X}}^k\}_{k=1}^K$ , are induced by a given feature map  $g : \mathcal{X} \rightarrow \mathcal{Z}$  applied to the measures of source domains  $\{\mathbb{P}_{\mathcal{X}}^k\}_{k=1}^K$ . Specifically,  $g_{\#} \mathbb{P}_{\mathcal{X}}^k(E) = \mathbb{P}_{\mathcal{X}}^k \circ g^{-1}(E)$  for any Borel set  $E$  on  $\mathcal{Z}$ .

However, defining feature measures for doubly residual architectures presents subtle challenges, as discussed in Section 3.2. These architectures include multiple feature extractors in  $\Psi = \{\psi^m\}_{m=1}^M$  as defined in (2), where each extractor  $\psi^m$  takes a sampled input passing through the residual operations of previous stacks. Within each stack, the input is repeatedly processed.

Moreover, unlike classification tasks with finite-dimensional output, residual architectures operate in an infinite-dimensional space  $\mathcal{Y}$  due to sequential data. This can lead to the scaling issues when training with highly distinct source domains. Additionally, the scaling factor may represent instance-wise characteristics, as observed in the numerical magnitudes of  $s$  values in Section 3.1, which exhibit noticeable variations in resolutions. Given these complexities, defining feature measures in a single shot is intricate for such architectures.

To resolve these issues, we propose a stack-wise alignment of feature measures on the subspace  $\tilde{\mathcal{Z}} \subseteq \mathcal{Z}$ . This alignment involves calculating measures for each stack using the multiple compositions of feature extractions in  $\Psi = \{\psi^m\}_{m=1}^M$ , backcasting operators in  $\Xi_{\uparrow} = \{\xi_{\uparrow}^m\}_{m=1}^M$  based on the residual principle described in (2), and a normalizing function  $\sigma : \mathcal{Z} \rightarrow \tilde{\mathcal{Z}}$ .

**Definition 4.1.** *The set of marginal feature measures in the  $m$ -th stack is defined by*

$$\{(\sigma \circ g^m)_{\#} \mathbb{P}_{\mathcal{X}}^k\}_{k=1}^K, \quad m = 1, \dots, M,$$

where each  $(\sigma \circ g^m)_{\#} \mathbb{P}_{\mathcal{X}}^k$  is a pushforward of  $\mathbb{P}_{\mathcal{X}}^k \in \{\mathbb{P}_{\mathcal{X}}^k\}_{k=1}^K$  induced by  $\sigma \circ g^m : \mathcal{X} \rightarrow \tilde{\mathcal{Z}}$ , and  $\sigma : \mathcal{Z} \rightarrow \tilde{\mathcal{Z}}$  is a normalizing function having  $C_{\sigma}$ -Lipschitz continuity (i.e.,  $\|\sigma(z) - \sigma(z')\| \leq C_{\sigma} \|z - z'\| \forall z, z' \in \mathcal{Z}$ ), and  $g^m : \mathcal{X} \rightarrow \mathcal{Z}$  is defined by

$$g^m(x) := (\psi^m \circ (r^m)^{(L-1)} \circ (r^{m-1})^{(L)} \circ \dots \circ (r^1)^{(L)})(x), \quad (5)$$

(with  $g^m = (\psi^m \circ (r^m)^{(L-1)})$  for  $m = 1$ ), and  $\psi^m : \mathcal{X} \rightarrow \mathcal{Z}$  is defined in (2), and  $r^m : \mathcal{X} \rightarrow \mathcal{X}$  is defined by

$$r^m(x) := x - (\xi_{\uparrow}^m \circ \psi^m)(x), \quad (6)$$

and  $(r^m)^{(L)}$  denotes  $L$ -times composition of  $r^m$  (with  $(r^m)^{(L-1)}(x) := x$  for  $L - 1 = 0$ ).

**Remark 4.1.**  $\sigma$  serves the purpose of enabling the model to learn invariant features by mitigating the influence of instance-wise characteristics associated with the scale information of each domain. Additionally, the Lipschitz condition imposed on  $\sigma$  prevents gradient explosion during model updates. We present two examples of such functions: (1) softmax :  $\mathcal{Z} \rightarrow \tilde{\mathcal{Z}} = (0, 1)^\gamma$  with  $\text{softmax}(z)_j = e^{z_j} / \sum_{i=1}^{\gamma} e^{z_i}$ ,  $j = 1, \dots, \gamma$ , and (2) tanh (hyperbolic tangent):  $\mathcal{Z} \rightarrow \tilde{\mathcal{Z}} = (-1, 1)^\gamma$  with  $\text{tanh}(z)_j = (e^{2z_j} - 1) / (e^{2z_j} + 1)$ ,  $j = 1, \dots, \gamma$ . Both functions are 1-Lipschitz continuous, i.e.,  $C_\sigma = 1$ . In Appendix E.3., we provide the ablation study under these functions, in addition to the case without the normalization.

If the feature alignment were embedded block-wise for every stack, the recurrent operation of the same block within each stack would derive a redundant gradient flow, which leads to exploding or vanishing gradients for long-term forecasting problems [36]. The proposed stack-wise feature alignment can mitigate such issues by sparsely propagating loss. Moreover, it can bring the interpretability of the original N-BEATS [34] by keeping the original stacking structure. Some heuristic demonstration for this argument is provided in Appendix E.1.

The operator  $g^m$  acts as an accumulated feature map up to the  $m$ -th stack, incorporating the previous  $m - 1$  backcasting residual operations for  $x \sim \mathbb{P}_{\mathcal{X}}^k \in \mathcal{P}(\mathcal{X})$ . Despite involving the intricate composition of  $\Psi$  and  $\Xi_{\uparrow}$ , the fully-connected layers within  $\Psi$  and  $\Xi_{\uparrow}$  exhibit Lipschitz continuity, ensuring the Lipschitz continuity of  $g^m$ . The Lipschitz constants of fully-connected layers are explicitly provided in [43, Section 6]. From this and Remark 4.1, we state the following lemma. The proof is provided in Appendix A.:

**Lemma 4.1.** For each  $m = 1, \dots, M$ , let  $C_m > 0$  and  $C_{m,\uparrow} > 0$  be Lipschitz constants of  $\psi^m$  and  $\xi_{\uparrow}^m$ , respectively. Then  $(\sigma \circ g^m)$  is  $C_{\sigma \circ g^m}$ -Lipschitz continuous with  $C_{\sigma \circ g^m} := C_\sigma C_m (1 + C_m, C_{m,\uparrow})^{L-1} \prod_{n=1}^{m-1} (1 + C_n C_{n,\uparrow})^L > 0$  for  $m = 2, \dots, M$ ,  $C_{\sigma \circ g^m} := C_\sigma C_m (1 + C_m, C_{m,\uparrow})^{L-1}$  for  $m = 1$ , and  $C_\sigma > 0$  in Definition 4.1).

Due to the residual principle (see Section 3.2), the accumulated feature maps  $\{g^m\}_{m=1}^M$  are nonseparable for  $\Psi$  and  $\Xi_{\uparrow}$ . So stack-wise alignment of marginal feature measures via regularizing  $\{g^m\}_{m=1}^M$  potentially deteriorates the backcasting power of  $\Xi_{\uparrow}$ , which could ultimately lead to prediction degrading of the model. Instead, we conduct the alignment by regularizing exclusively on feature extractors  $\Psi$ . More precisely, we propose a stack-wise alignment of marginal feature measures (defined in Definition 4.1) as the following optimization: for any given  $\Xi_{\uparrow} = \{\xi_{\uparrow}^m\}_{m=1}^M$ ,

$$\inf_{\Psi} \left\{ \sum_{m=1}^M \max_{i,j \in \{1, \dots, K\}, i \neq j} d((\sigma \circ g^m)_{\#} \mathbb{P}_{\mathcal{X}}^i, (\sigma \circ g^m)_{\#} \mathbb{P}_{\mathcal{X}}^j) \right\}, \quad (7)$$

where  $d(\cdot, \cdot) : \mathcal{P}(\tilde{\mathcal{Z}}) \times \mathcal{P}(\tilde{\mathcal{Z}}) \rightarrow \mathbb{R}_+$  denotes a divergence (or metric), which will be defined as an entropic regularized optimal transport distance in next section. The schematic illustration of the stack-wise alignment can be found in Figure 1 of Appendix A.

## 4.2 Sinkhorn divergence on input and latent spaces

In the generative adversarial framework [16, 3], optimal transport distances are common metrics used to train generators to induce pushforward measures close to a given target measure. Recently, [49] utilized an entropic regularized optimal transport distance [13, 14] to generate time series data. From these studies, we speculate that the entropic regularized one brings both learning invariant factors from the pushforward measures (in Definition 4.1) and the computational efficiency for high-dimensional sequential data. Specifically, we consider the regularized quadratic Wasserstein-2 distance on  $\tilde{\mathcal{Z}}$ : for any  $\epsilon \geq 0$

$$\mathcal{W}_{\epsilon, \tilde{\mathcal{Z}}}(\mu, \nu) := \inf_{\pi \in \Pi(\mu, \nu; \tilde{\mathcal{Z}})} \left\{ \int_{\tilde{\mathcal{Z}} \times \tilde{\mathcal{Z}}} \left( \|x - y\|^2 + \epsilon \log \left( \frac{d\pi(x, y)}{d\mu(x) d\nu(y)} \right) \right) d\pi(x, y) \right\}, \quad (8)$$

where  $\epsilon$  denotes the regularization degree and  $\Pi(\mu, \nu; \tilde{\mathcal{Z}})$  is the space of all couplings (or transportation plans) the marginals of which are respectively  $\mu, \nu \in \mathcal{P}(\tilde{\mathcal{Z}})$ . By replacing  $\tilde{\mathcal{Z}}$  with  $\mathcal{X}$  in (8), we further denote by  $\mathcal{W}_{\epsilon, \mathcal{X}}(\cdot, \cdot)$  the regularized quadratic Wasserstein-2 distance on  $\mathcal{X}$ .

Even if the residual architecture induces the intricate representation learning procedure (see Section 4.1), the proposed stack-wise alignment of the pushforward measures via (8) is well-defined and feasible provided that the pair-wise divergence of source domains' measures under the same distance is empirically manageable. By using the duality of the regularized optimal transport distance in [37, Remark 4.18 in Section 4.4] and the Lipschitz continuity of  $\{\sigma \circ g^m\}_{m=1}^M$  (see Lemma 4.1), we provide the following theorem, which supports this claim. The proof is provided in Appendix B.

**Theorem 4.1.** *For any  $\epsilon \geq 0$ , the following holds*

$$\sum_{m=1}^M \max_{i, j \in \{1, \dots, K\}, i \neq j} \mathcal{W}_{\epsilon, \tilde{\mathcal{Z}}}((\sigma \circ g^m)_{\#} \mathbb{P}_{\mathcal{X}}^i, (\sigma \circ g^m)_{\#} \mathbb{P}_{\mathcal{X}}^j) \leq C \max_{i, j \in \{1, \dots, K\}, i \neq j} \mathcal{W}_{\epsilon, \mathcal{X}}(\mathbb{P}_{\mathcal{X}}^i, \mathbb{P}_{\mathcal{X}}^j),$$

with  $C := \sum_{m=1}^M \max\{(C_{\sigma \circ g^m})^2, 1\} > 0$  and  $C_{\sigma \circ g^m} > 0$  defined in Lemma 4.1.

In [33, Lemma 3, Proposition 6], learning bounds for the maximum mean discrepancy (MMD) and the regularized distance (8) are investigated under a single-layered fully connected network. While the upper bound in Theorem 4.1 provides a similar learning bound for the distance (8), it demonstrates that the stack-wise alignment (7) via the regularized Wasserstein distance can be embedded into the intricate residual stacking architecture with the deep layered network. While the Lipschitz continuity of  $\{\sigma \circ g^m\}_{m=1}^M$  (see Lemma 4.1) allows to have a nice bound, there exists room for having a tighter bound by deriving the smallest Lipschitz constant [43] and applying the spectral normalization [30], which will be left for the future extension.

The entropic term attached with  $\epsilon$  in (8) is supposed to improve computational stability of the classical optimal transport distance, whereas it causes a bias on the estimator for the (empirical) regularized Wasserstein distance. To mitigate this issue, according to [9], we adopt the following debiased version of the regularized distance (8), which is referred to as the Sinkhorn divergence: for any given  $\epsilon \geq 0$ ,

$$\widehat{\mathcal{W}}_{\epsilon, \tilde{\mathcal{Z}}}(\mu, \nu) := \mathcal{W}_{\epsilon, \tilde{\mathcal{Z}}}(\mu, \nu) - \frac{1}{2}(\mathcal{W}_{\epsilon, \tilde{\mathcal{Z}}}(\nu, \nu) + \mathcal{W}_{\epsilon, \tilde{\mathcal{Z}}}(\mu, \mu)) \quad \forall \mu, \nu \in \mathcal{P}(\tilde{\mathcal{Z}}). \quad (9)$$

In our algorithm, the feature alignment is realized by minimizing Sinkhorn divergences (with denoting  $d(\cdot, \cdot) = \widehat{\mathcal{W}}_{\epsilon, \tilde{\mathcal{Z}}}(\cdot, \cdot)$  in (7)) between (empirical) marginal feature measures.

### 4.3 Training objective and algorithm

We now combine the results in Sections 4.1 and 4.2 to formulate the feature-aligned N-BEATS algorithm. To that end, we first represent all the residual operators in  $\Psi$ ,  $\Xi_{\downarrow}$ , and  $\Xi_{\uparrow}$  (in Section 3.2) as parameterized forms  $\Psi(\Phi) = \{\psi^m(\cdot; \phi_m)\}_{m=1}^M$ ,  $\Xi_{\downarrow}(\Theta_{\downarrow}) = \{\xi_{\downarrow}^m(\cdot; \theta_{m, \downarrow})\}_{m=1}^M$ ,  $\Xi_{\uparrow}(\Theta_{\uparrow}) = \{\xi_{\uparrow}^m(\cdot; \theta_{m, \uparrow})\}_{m=1}^M$  respectively, with parameters sets  $\Phi := \{\phi_m\}_{m=1}^M$ ,  $\Theta_{\downarrow} := \{\theta_{m, \downarrow}\}_{m=1}^M$ , and  $\Theta_{\uparrow} := \{\theta_{m, \uparrow}\}_{m=1}^M$  denoting weights of the fully connected neural networks.

In terms of the parameters sets, we provide the following functional

$$\mathbf{L}_{\lambda}(\Phi, \Theta_{\downarrow}, \Theta_{\uparrow}) := \mathcal{L}(\mathfrak{F}(\Phi, \Theta_{\downarrow}, \Theta_{\uparrow})) + \lambda \mathcal{L}_{\text{align}}(\Phi, \Theta_{\uparrow}), \quad (10)$$

where  $\mathcal{L}(\mathfrak{F}(\cdot, \cdot, \cdot))$  denotes the forecasting loss functional from (1) and  $\mathcal{L}_{\text{align}}(\cdot, \cdot)$  representing the feature alignment (7) with the Sinkhorn divergence (9) is given by

$$\mathcal{L}_{\text{align}}(\Phi, \Theta_{\uparrow}) := \sum_{m=1}^M \max_{i, j \in \{1, \dots, K\}, i \neq j} \widehat{\mathcal{W}}_{\epsilon, \tilde{\mathcal{Z}}}((\sigma \circ g_{\Phi, \Theta_{\uparrow}}^m)_{\#} \mathbb{P}_{\mathcal{X}}^i, (\sigma \circ g_{\Phi, \Theta_{\uparrow}}^m)_{\#} \mathbb{P}_{\mathcal{X}}^j), \quad (11)$$

and  $g_{\Phi, \Theta_{\uparrow}}^m := g^m(\cdot; \{\phi_n\}_{n=1}^m, \{\theta_{n, \uparrow}\}_{n=1}^m)$ ,  $m = 1, \dots, M$ , denotes the parameterized version of  $g^m$ .

To update  $(\Phi, \Theta_{\downarrow}, \Theta_{\uparrow})$  and the corresponding gradient using a mini-batch, we approximate each  $\widehat{\mathcal{W}}_{\epsilon, \tilde{\mathcal{Z}}}((\sigma \circ g_{\Phi, \Theta_{\uparrow}}^m)_{\#} \mathbb{P}_{\mathcal{X}}^i, (\sigma \circ g_{\Phi, \Theta_{\uparrow}}^m)_{\#} \mathbb{P}_{\mathcal{X}}^j)$  as its empirical counterpart  $\widehat{\mathcal{W}}_{\epsilon, \tilde{\mathcal{Z}}}(\mu_{\Phi, \Theta_{\uparrow}}^{m, (i)}, \mu_{\Phi, \Theta_{\uparrow}}^{m, (j)})$ , where the empirical measure is given by  $\mu_{\Phi, \Theta_{\uparrow}}^{m, (k)} := \frac{1}{B} \sum_{b=1}^B \delta_{\tilde{z}_b^{(k)}}$ , with  $\tilde{z}_b^{(k)} := \sigma \circ g_{\Phi, \Theta_{\uparrow}}^m(x_b^{(k)})$  and

$\{(x_b^{(k)}, y_b^{(k)})\}_{b=1}^B$  from  $\mathcal{D}^k$ , and  $B$  and  $\delta_z$  denoting mini-batch size and the Dirac measure centered on  $z \in \tilde{\mathcal{Z}}$ , respectively.

As we mentioned in Section 4.1, the feature alignment of marginal feature distributions is realized by optimizing  $\Phi$ , though  $\{g_{\Phi, \Theta_{\uparrow}}^m\}_{m=1}^M$  are non-separable for  $\Phi$  and  $\Theta_{\uparrow}$ . At the same time, the forecasting objective (1) should be minimized by optimizing  $(\Phi, \Theta_{\downarrow}, \Theta_{\uparrow})$ . To bring these two components together, we adopt the following alternate optimization inspired from [11, Section 3.1]:

$$\Theta_{\downarrow}^*, \Theta_{\uparrow}^* := \arg \min_{\Theta_{\downarrow}, \Theta_{\uparrow}} \mathcal{L}(\mathfrak{F}(\Phi^*, \Theta_{\downarrow}, \Theta_{\uparrow})) \quad \text{and} \quad \Phi^* := \arg \min_{\Phi} \mathbf{L}_{\lambda}(\Phi, \Theta_{\downarrow}^*, \Theta_{\uparrow}^*) \quad (12)$$

The training procedure with this optimization is summarized in Algorithm 1.

---

**Algorithm 1:** training Feature-aligned N-BEATS

---

**Requires :**  $\eta$  (learning rate),  $B$  (mini-batch size);

```

1 Initialize  $\Phi, \Theta_{\downarrow}, \Theta_{\uparrow}$ ;
2 while not converged do
3   Sample  $\{(x_1^{(k)}, y_1^{(k)}), \dots, (x_B^{(k)}, y_B^{(k)})\}$  from  $\mathcal{D}^k$  for each  $k = 1, \dots, K$ ;
4   Initialize  $\{\hat{y}_1^{(k)}, \dots, \hat{y}_B^{(k)}\} \leftarrow \{0, \dots, 0\}$  for each  $k = 1, \dots, K$ ;
5   for  $m = 1$  to  $M$  do
6     for  $k = 1$  to  $K$  do
7       Compute  $\{g_{\Phi, \Theta_{\uparrow}}^m(x_1^{(k)}), \dots, g_{\Phi, \Theta_{\uparrow}}^m(x_B^{(k)})\}$ ;
8        $\hat{y}_b^{(k)} \leftarrow \hat{y}_b^{(k)} + \xi_{\downarrow}^m(g_{\Phi, \Theta_{\uparrow}}^m(x_b^{(k)}); \theta_{m, \downarrow}) \forall b = 1, \dots, B$ ;
9     end
10    end
11    Compute  $\mu_{\Phi, \Theta_{\uparrow}}^{m, (k)}$  for each  $m = 1, \dots, M$  and  $k = 1, \dots, K$ ;
12    Update  $\Phi$  based on  $\lambda \mathcal{L}_{\text{align}}(\cdot, \Theta_{\uparrow})$ , i.e., for each  $m = 1, \dots, M$ ,
13     $\phi_m \leftarrow \phi_m + \eta \nabla_{\phi_m} \left( \lambda \sum_{n=1}^M \max_{i, j \in \{1, \dots, K\}, i \neq j} \widehat{\mathcal{W}}_{\epsilon, \tilde{\mathcal{Z}}} \left( \mu_{\Phi, \Theta_{\uparrow}}^{n, (i)}, \mu_{\Phi, \Theta_{\uparrow}}^{n, (j)} \right) \right)$ ;
14    Update  $(\Phi, \Theta_{\downarrow}, \Theta_{\uparrow})$  based on  $\mathcal{L}(\mathfrak{F}(\cdot, \cdot, \cdot))$ , i.e., for each  $m = 1, \dots, M$ ,
15     $(\{\phi_m, \theta_{m, \downarrow}, \theta_{m, \uparrow}\} \leftarrow (\phi_m, \theta_{m, \downarrow}, \theta_{m, \uparrow}) + \eta \frac{1}{K \cdot B} \sum_{k=1}^K \sum_{b=1}^B \nabla_{(\phi_m, \theta_{m, \downarrow}, \theta_{m, \uparrow})} l(\hat{y}_b^{(k)}, y_b^{(k)})$ ;
16 end

```

---

## 5 Experiments

### 5.1 Evaluation Protocol

To comprehensively evaluate the proposed approach and capture semantic diversity among domains, we define a set of semantically similar domains called the *superdomain*  $\mathcal{A}$ . The evaluation scenarios are categorized into *in-domain generalization* (IDG), *cross-domain generalization* (CDG), and *out-domain generalization* (ODG) as follows: (1) IDG:  $\mathcal{D} \subset \mathcal{A}_i, \mathcal{D}^T \in \mathcal{A}_i$ ; (2) CDG:  $\{\mathcal{D}^k\}_{k=1}^{\kappa-1} \subset \mathcal{A}_i, \{\mathcal{D}^k\}_{k=\kappa}^K \subset \mathcal{A}_j, \mathcal{D}^T \in \mathcal{A}_i$  where  $i \neq j, 1 < \kappa \leq K$ ; (3) ODG:  $\mathcal{D} \subset \mathcal{A}_i, \mathcal{D}^T \in \mathcal{A}_j$  where  $i \neq j$ .

We construct a dataset consisting of two superdomains: **finance** and **weather**. Each superdomain comprises four subordinate domains: **finance** includes **commodity**, **income**, **interest rate**, and **exchange rate**, while **weather** includes **pressure**, **rain**, **temperature**, and **wind**. We collect financial data from the Federal Reserve Bank of St. Louis (FRED)<sup>3</sup>, and weather data from the National Oceanic and Atmospheric Administration (NOAA)<sup>4</sup>. It is worth noting that our dataset consists entirely of real-world data and covers a wide range of frequencies, including daily, weekly, monthly, quarterly, and yearly observations. We randomly split each domain into three sets: 70% for training, 10% for validation, and 20% for testing. To isolate the effects solely attributed to domain shift, we ensure that the number of data points for each domain is fixed at 7,500. For detailed data configuration, refer to Appendix D.1.

<sup>3</sup><https://fred.stlouisfed.org>

<sup>4</sup><https://ncei.noaa.gov>

Table 1: **Domain generalization performance.** For each target domain, we conduct experiments by averaging the different combinations of source domains (1 for IDG, 4 for ODG, and 18 for CDG). FA denotes feature alignment. All experiments are repeated three times with different random seeds, and we report the mean results.

Method		N-HITS		+ FA (ours)		N-BEATS-I		+ FA (ours)		N-BEATS-G		+ FA (ours)	
Metric		SMAPE	MASE	SMAPE	MASE	SMAPE	MASE	SMAPE	MASE	SMAPE	MASE	SMAPE	MASE
<i>In-domain Generalization</i>													
FRED	Commodity	0.083	0.045	<b>0.068</b>	<b>0.043</b>	<b>0.125</b>	0.053	0.126	0.053	0.165	0.143	<b>0.080</b>	<b>0.044</b>
	Income	0.299	0.058	<b>0.297</b>	<b>0.054</b>	0.305	0.055	<b>0.302</b>	0.055	0.301	0.056	<b>0.298</b>	<b>0.055</b>
NOAA	Interest rate	0.072	0.081	<b>0.071</b>	0.081	0.088	<b>0.084</b>	<b>0.086</b>	0.091	0.080	0.083	<b>0.074</b>	<b>0.081</b>
	Exchange rate	0.024	0.051	0.024	<b>0.050</b>	<b>0.028</b>	0.056	0.029	0.056	0.025	0.051	<b>0.024</b>	<b>0.050</b>
	Pressure	0.394	0.276	<b>0.384</b>	<b>0.272</b>	0.392	0.266	<b>0.389</b>	<b>0.263</b>	0.384	0.276	0.384	0.276
	Rain	1.776	1.211	<b>1.776</b>	<b>1.208</b>	<b>1.792</b>	<b>2.922</b>	1.805	3.046	1.818	1.690	<b>1.776</b>	<b>1.208</b>
	Temperature	0.247	0.242	0.247	0.242	0.234	0.231	<b>0.231</b>	<b>0.227</b>	0.247	0.242	<b>0.245</b>	<b>0.241</b>
	Wind	0.455	0.641	<b>0.452</b>	<b>0.640</b>	<b>0.433</b>	<b>0.622</b>	0.434	0.623	0.454	0.641	<b>0.452</b>	<b>0.640</b>
	Average	0.419	0.326	<b>0.415</b>	<b>0.324</b>	0.426	<b>0.537</b>	<b>0.424</b>	0.551	0.434	0.398	<b>0.417</b>	<b>0.325</b>
	<i>Cross-domain Generalization</i>												
FRED	Commodity	0.082	0.047	<b>0.081</b>	<b>0.044</b>	<b>0.195</b>	0.060	0.197	<b>0.059</b>	0.119	0.046	<b>0.107</b>	0.046
	Income	0.296	0.054	<b>0.295</b>	<b>0.053</b>	0.327	0.072	<b>0.323</b>	<b>0.070</b>	0.301	0.055	<b>0.295</b>	<b>0.053</b>
NOAA	Interest rate	0.086	0.074	<b>0.085</b>	0.074	0.146	<b>0.051</b>	0.146	0.054	0.102	0.077	<b>0.100</b>	0.077
	Exchange rate	0.032	0.056	<b>0.029</b>	<b>0.055</b>	<b>0.054</b>	0.074	0.055	<b>0.063</b>	0.032	0.056	<b>0.031</b>	<b>0.055</b>
	Pressure	0.375	0.264	<b>0.372</b>	<b>0.260</b>	0.408	0.307	<b>0.405</b>	<b>0.299</b>	0.540	0.374	<b>0.372</b>	<b>0.263</b>
	Rain	1.807	1.169	<b>1.803</b>	<b>0.783</b>	1.800	2.091	<b>1.787</b>	<b>1.831</b>	1.807	<b>1.169</b>	<b>1.804</b>	1.178
	Temperature	0.334	0.243	<b>0.245</b>	<b>0.242</b>	0.275	0.245	<b>0.240</b>	<b>0.244</b>	0.253	0.245	<b>0.245</b>	<b>0.243</b>
	Wind	0.453	0.643	<b>0.452</b>	0.643	0.441	0.646	<b>0.439</b>	0.646	0.453	0.643	<b>0.452</b>	0.643
	Average	0.433	0.318	<b>0.420</b>	<b>0.269</b>	0.456	0.443	<b>0.449</b>	<b>0.408</b>	0.450	0.333	<b>0.426</b>	<b>0.319</b>
	<i>Out-domain Generalization</i>												
FRED	Commodity	0.136	0.049	<b>0.103</b>	<b>0.046</b>	0.279	0.072	<b>0.258</b>	<b>0.069</b>	0.195	0.052	<b>0.136</b>	<b>0.049</b>
	Income	0.299	0.057	<b>0.298</b>	<b>0.055</b>	0.369	0.082	<b>0.335</b>	<b>0.075</b>	0.305	0.056	<b>0.304</b>	<b>0.055</b>
NOAA	Interest rate	0.120	0.074	<b>0.100</b>	<b>0.070</b>	0.200	<b>0.044</b>	<b>0.189</b>	0.046	0.148	0.073	<b>0.120</b>	0.073
	Exchange rate	0.035	0.059	<b>0.034</b>	<b>0.058</b>	0.078	0.078	<b>0.075</b>	<b>0.069</b>	0.040	0.062	<b>0.039</b>	<b>0.060</b>
	Pressure	0.368	0.255	<b>0.350</b>	<b>0.250</b>	0.759	0.396	<b>0.409</b>	<b>0.305</b>	0.368	0.255	<b>0.367</b>	0.255
	Rain	1.821	1.099	<b>1.804</b>	<b>0.910</b>	1.798	1.600	<b>1.793</b>	<b>1.430</b>	1.818	1.100	<b>1.806</b>	<b>0.918</b>
	Temperature	0.247	0.245	<b>0.245</b>	<b>0.243</b>	0.247	0.353	<b>0.246</b>	<b>0.255</b>	0.247	0.245	<b>0.246</b>	<b>0.244</b>
	Wind	0.455	0.645	<b>0.454</b>	<b>0.644</b>	0.451	0.665	<b>0.449</b>	<b>0.662</b>	0.455	0.645	<b>0.454</b>	0.645
	Average	0.436	0.310	<b>0.424</b>	<b>0.182</b>	0.523	0.412	<b>0.469</b>	<b>0.364</b>	0.447	0.310	<b>0.433</b>	<b>0.287</b>

\* Smaller values of the error metrics SMAPE and MASE indicate better performance.

To evaluate IDG, we designate one target domain and consider the remaining domains within the same superdomain as source domains, e.g.,  $\mathcal{D} = \{\text{pressure, rain, temperature}\}$ , and  $\mathcal{D}^T = \text{wind}$ . To fair comparisons, we standardize the number of source domains to three across all CDG and ODG scenarios. In CDG, we select one domain from the superdomain of the target domain and two domains from the other superdomain as the source, e.g.,  $\mathcal{D} = \{\text{commodity, income, pressure}\}$ , and  $\mathcal{D}^T = \text{rain}$ . ODG scenarios involve no overlap between the source and target domains in terms of  $\mathcal{A}$ , e.g.,  $\mathcal{D} = \{\text{pressure, rain, temperature}\}$ , and  $\mathcal{D}^T = \text{commodity}$ .

We compare the performance of our approach against two N-BEATS [34] derived models: N-BEATS-G and N-BEATS-I. Additionally, we evaluate the performance of N-HITS [7], an improved version of N-BEATS that has exhibited notable advancements in recent studies. Our experimental setup is motivated by two avenues of research on time series forecasting: (1) the limitations of methods based on transformer architectures [50], and (2) the effectiveness of doubly residual stacking networks for generalization [35]. To ensure a fair and thorough comparison, we carefully fine-tune all models and their hyperparameters. We conduct a grid search over a wide range of hyperparameter values and select the optimal settings based on their performance on the validation set.

## 5.2 Experimental Details

We adopt the symmetric mean absolute percentage error (sMAPE) metric as the prediction loss function  $\mathcal{L}$  (10). The softmax function is employed as normalizing function  $\sigma$ . The hyperparameters are set as follows:  $M = 3$ ,  $L = 4$ ,  $\alpha = 50$ ,  $\beta = 10$ , and  $\gamma = 512$ . We utilize the Adam optimizer [21] for optimization and determine the learning rate, including initial value and scheduling strategy, stopping criterion, and batch size through grid search. Additional implementation details are provided in Appendix D.2.

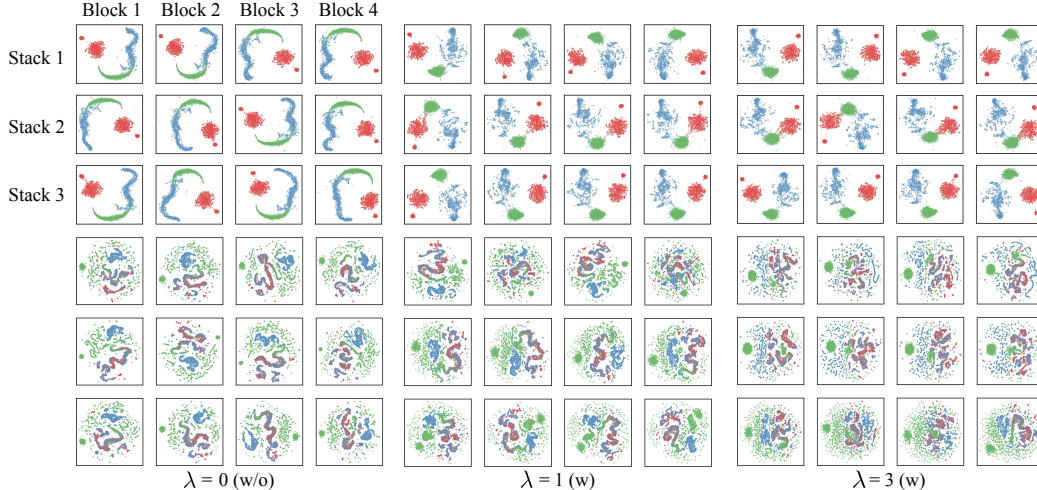


Figure 1: **Visual comparison between with alignment (w) and without alignment (w/o).** In the first scenario, alignment is visible as green and red instances are connected (especially when  $\lambda = 3$ ). In the other scenario, instances are dispersed, particularly with increased dispersion of blue instances in the first and second stacks at  $\lambda = 3$ , resulting in heightened entropy between domains.

### 5.3 Experimental Results and Analysis

We evaluate the performance using the *SMAPE* and *MASE* metrics, which are defined in Appendix D.3. Table 1 shows that incorporating feature alignment into the deep residual stacking architecture models improves their generalizability, resulting in better performance across most of the experiments. However, our framework demonstrates the least impact on N-BEATS-I. This may be due to limitations in the seasonality and trend-capturing modules of N-BEATS-I in effectively capturing diverse frequencies. Furthermore, the alignment of misrepresented feature distributions does not seem to provide significant benefits. For further qualitative analysis, please refer to Appendix F.1.

To visualize the representations, i.e., samples of marginal feature measures, observed from N-BEATS-G with and without alignment, we use the uniform manifold approximation and projection (UMAP) technique [29]. In order to mitigate the influence of unaligned scale information, we use the softmax function to remove the scale information and analyze the semantic relationship between domains. Figure 1 highlights two noticeable trends: (1) instances are positioned closer to each other, and (2) the entropy of domains exhibits a significant increase. For comprehensive visual analyses on N-BEATS-I and N-HiTS, please refer to Appendix F.2.

**Further Analysis.** We conduct a series of supplementary experiments to delve deeper into the effectiveness of our approach. These experiments encompass the following investigations: (1) Comparison between block-wise and stack-wise feature alignment. (2) Exploration of additional distance metrics for the feature alignment. (3) Comparison of several normalizing functions. (4) Analysis of the impact of our approach in the presence of subtle domain shifts. Comprehensive details and information on these experiments can be found in Appendix E.

## 6 Conclusion

In this work, we propose Feature-aligned N-BEATS, a domain generalization model that combines the doubly residual stacking architecture of N-BEATS [34] with feature alignment techniques in representation learning theory. Our model leverages on stack-wise feature alignment, which takes into account domain-invariant learning and the interpretability of N-BEATS. Extensive experimental analysis indicates that Feature-aligned N-BEATS achieves remarkable generalization performance across different domains. Moving forward, potential future directions are to enhance stability of the model through the spectral normalization [30] on residual operators and to extend into conditional feature alignment [23, 52] within the residual architecture.

**Acknowledgement.** M. Kang was supported by the NRF grant[2012R1A2C3010887] and the MSIT/IITP([1711117093], [NO.2021-0-00077], [No. 2021-0-01343, Artificial Intelligence Graduate School Program(SNU)]). K. Park acknowledges the support of the Presidential Postdoctoral Fellowship of Nanyang Technological University.

## References

- [1] I. Albuquerque, J. Monteiro, M. Darvishi, T. H. Falk, and I. Mitliagkas. Generalizing to unseen domains via distribution matching. *arXiv preprint arXiv:1911.00804*, 2019.
- [2] L. Ambrosio, N. Gigli, and G. Savaré. *Gradient flows: in metric spaces and in the space of probability measures*. Springer Science & Business Media, 2005.
- [3] M. Arjovsky, S. Chintala, and L. Bottou. Wasserstein generative adversarial networks. In *International Conference on Machine Learning*, pages 214–223. PMLR, 2017.
- [4] K. Bandara, C. Bergmeir, and S. Smyl. Forecasting across time series databases using recurrent neural networks on groups of similar series: A clustering approach. *Expert Systems with Applications*, 140:112896, 2020.
- [5] Y. Bengio, A. Courville, and P. Vincent. Representation learning: A review and new perspectives. *IEEE Transactions on Pattern Analysis and Machine Intelligence*, 35(8):1798–1828, 2013.
- [6] W. Cao, D. Wang, J. Li, H. Zhou, L. Li, and Y. Li. Brits: Bidirectional recurrent imputation for time series. *Advances in Neural Information Processing Systems*, 31, 2018.
- [7] C. Challu, K. G. Olivares, B. N. Oreshkin, F. Garza, M. Mergenthaler, and A. Dubrawski. N-hits: Neural hierarchical interpolation for time series forecasting. *arXiv preprint arXiv:2201.12886*, 2022.
- [8] Y. Chen, Y. Kang, Y. Chen, and Z. Wang. Probabilistic forecasting with temporal convolutional neural network. *Neurocomputing*, 399:491–501, 2020.
- [9] L. Chizat, P. Roussillon, F. Léger, F.-X. Vialard, and G. Peyré. Faster wasserstein distance estimation with the sinkhorn divergence. *Advances in Neural Information Processing Systems*, 33:2257–2269, 2020.
- [10] H. Federer. *Geometric measure theory*. Springer, 2014.
- [11] Y. Ganin and V. Lempitsky. Unsupervised domain adaptation by backpropagation. In *International Conference on Machine Learning*, pages 1180–1189. PMLR, 2015.
- [12] Y. Ganin, E. Ustinova, H. Ajakan, P. Germain, H. Larochelle, F. Laviolette, M. Marchand, and V. Lempitsky. Domain-adversarial training of neural networks. *The Journal of Machine Learning Research*, 17(1):2096–2030, 2016.
- [13] A. Genevay, M. Cuturi, G. Peyré, and F. Bach. Stochastic optimization for large-scale optimal transport. *Advances in Neural Information Processing Systems*, 29, 2016.
- [14] A. Genevay, G. Peyré, and M. Cuturi. Learning generative models with sinkhorn divergences. In *International Conference on Artificial Intelligence and Statistics*, pages 1608–1617. PMLR, 2018.
- [15] S. Ghimire, A. Masoomi, and J. Dy. Reliable estimation of kl divergence using a discriminator in reproducing kernel hilbert space. *Advances in Neural Information Processing Systems*, 34:10221–10233, 2021.
- [16] I. Goodfellow, J. Pouget-Abadie, M. Mirza, B. Xu, D. Warde-Farley, S. Ozair, A. Courville, and Y. Bengio. Generative adversarial networks. *Communications of the ACM*, 63(11):139–144, 2020.
- [17] A. Gretton, K. M. Borgwardt, M. J. Rasch, B. Schölkopf, and A. Smola. A kernel two-sample test. *The Journal of Machine Learning Research*, 13(1):723–773, 2012.
- [18] H. Hewamalage, C. Bergmeir, and K. Bandara. Recurrent neural networks for time series forecasting: Current status and future directions. *International Journal of Forecasting*, 37(1):388–427, 2021.
- [19] H. Hu, M. Tang, and C. Bai. Datsing: Data augmented time series forecasting with adversarial domain adaptation. In *Proceedings of the ACM International Conference on Information & Knowledge Management*, pages 2061–2064, 2020.
- [20] X. Jin, Y. Park, D. Maddix, H. Wang, and Y. Wang. Domain adaptation for time series forecasting via attention sharing. In *International Conference on Machine Learning*, pages 10280–10297. PMLR, 2022.
- [21] D. P. Kingma and J. Ba. Adam: A method for stochastic optimization. *arXiv preprint arXiv:1412.6980*, 2014.
- [22] H. Li, S. J. Pan, S. Wang, and A. C. Kot. Domain generalization with adversarial feature learning. In *Proceedings of the IEEE Conference on Computer Vision and Pattern Recognition*, pages 5400–5409, 2018.

- [23] Y. Li, X. Tian, M. Gong, Y. Liu, T. Liu, K. Zhang, and D. Tao. Deep domain generalization via conditional invariant adversarial networks. In *Proceedings of the European Conference on Computer Vision*, pages 624–639, 2018.
- [24] Z. Li, R. Cai, J. Chen, Y. Yan, W. Chen, K. Zhang, and J. Ye. Time-series domain adaptation via sparse associative structure alignment: Learning invariance and variance. *arXiv preprint arXiv:2205.03554*, 2022.
- [25] B. Lim, S. Ö. Arık, N. Loeff, and T. Pfister. Temporal fusion transformers for interpretable multi-horizon time series forecasting. *International Journal of Forecasting*, 37(4):1748–1764, 2021.
- [26] M. Liu, A. Zeng, M. Chen, Z. Xu, Q. Lai, L. Ma, and Q. Xu. Scinet: time series modeling and forecasting with sample convolution and interaction. *Advances in Neural Information Processing Systems*, 35:5816–5828, 2022.
- [27] K. Madhusudhanan, J. Burchert, N. Duong-Trung, S. Born, and L. Schmidt-Thieme. Yformer: U-net inspired transformer architecture for far horizon time series forecasting. *arXiv preprint arXiv:2110.08255*, 2021.
- [28] T. Matsuura and T. Harada. Domain generalization using a mixture of multiple latent domains. In *Proceedings of the AAAI Conference on Artificial Intelligence*, volume 34, pages 11749–11756, 2020.
- [29] L. McInnes, J. Healy, and J. Melville. Umap: Uniform manifold approximation and projection for dimension reduction. *arXiv preprint arXiv:1802.03426*, 2018.
- [30] T. Miyato, T. Kataoka, M. Koyama, and Y. Yoshida. Spectral normalization for generative adversarial networks. *arXiv preprint arXiv:1802.05957*, 2018.
- [31] K. Muandet, D. Balduzzi, and B. Schölkopf. Domain generalization via invariant feature representation. In *International Conference on Machine Learning*, pages 10–18. PMLR, 2013.
- [32] V. Nair and G. E. Hinton. Rectified linear units improve restricted boltzmann machines. In *International Conference on Machine Learning*, pages 807–814, 2010.
- [33] L. Oneto, M. Donini, G. Luise, C. Ciliberto, A. Maurer, and M. Pontil. Exploiting mmd and sinkhorn divergences for fair and transferable representation learning. *Advances in Neural Information Processing Systems*, 33:15360–15370, 2020.
- [34] B. N. Oreshkin, D. Carпов, N. Chapados, and Y. Bengio. N-beats: Neural basis expansion analysis for interpretable time series forecasting. *arXiv preprint arXiv:1905.10437*, 2019.
- [35] B. N. Oreshkin, D. Carпов, N. Chapados, and Y. Bengio. Meta-learning framework with applications to zero-shot time-series forecasting. In *Proceedings of the AAAI Conference on Artificial Intelligence*, volume 35, pages 9242–9250, 2021.
- [36] R. Pascanu, T. Mikolov, and Y. Bengio. On the difficulty of training recurrent neural networks. In *International Conference on Machine Learning*, pages 1310–1318. Pmlr, 2013.
- [37] G. Peyré, M. Cuturi, et al. Computational optimal transport: With applications to data science. *Foundations and Trends® in Machine Learning*, 11(5-6):355–607, 2019.
- [38] J. Quinonero-Candela, M. Sugiyama, A. Schwaighofer, and N. D. Lawrence. *Dataset shift in machine learning*. Mit Press, 2008.
- [39] S. S. Rangapuram, M. W. Seeger, J. Gasthaus, L. Stella, Y. Wang, and T. Januschowski. Deep state space models for time series forecasting. *Advances in Neural Information Processing Systems*, 31, 2018.
- [40] D. Salinas, V. Flunkert, J. Gasthaus, and T. Januschowski. Deepar: Probabilistic forecasting with autoregressive recurrent networks. *International Journal of Forecasting*, 36(3):1181–1191, 2020.
- [41] C. Shui, B. Wang, and C. Gagné. On the benefits of representation regularization in invariance based domain generalization. *Machine Learning*, 111(3):895–915, 2022.
- [42] V. Vapnik. Principles of risk minimization for learning theory. *Advances in Neural Information Processing Systems*, 4, 1991.
- [43] A. Virmaux and K. Scaman. Lipschitz regularity of deep neural networks: analysis and efficient estimation. *Advances in Neural Information Processing Systems*, 31, 2018.
- [44] J. Wang, C. Lan, C. Liu, Y. Ouyang, T. Qin, W. Lu, Y. Chen, W. Zeng, and P. Yu. Generalizing to unseen domains: A survey on domain generalization. *IEEE Transactions on Knowledge and Data Engineering*, 2022.
- [45] M. Wang and W. Deng. Deep visual domain adaptation: A survey. *Neurocomputing*, 312:135–153, 2018.
- [46] G. Wilson, J. R. Doppa, and D. J. Cook. Multi-source deep domain adaptation with weak supervision for time-series sensor data. In *Proceedings of the ACM SIGKDD international conference on knowledge discovery & data mining*, pages 1768–1778, 2020.
- [47] G. Woo, C. Liu, D. Sahoo, A. Kumar, and S. Hoi. Etsformer: Exponential smoothing transformers for time-series forecasting. *arXiv preprint arXiv:2202.01381*, 2022.

- [48] H. Wu, J. Xu, J. Wang, and M. Long. Autoformer: Decomposition transformers with auto-correlation for long-term series forecasting. *Advances in Neural Information Processing Systems*, 34:22419–22430, 2021.
- [49] T. Xu, L. K. Wenliang, M. Munn, and B. Acciaio. Cot-gan: Generating sequential data via causal optimal transport. *Advances in Neural Information Processing Systems*, 33:8798–8809, 2020.
- [50] A. Zeng, M. Chen, L. Zhang, and Q. Xu. Are transformers effective for time series forecasting? *arXiv preprint arXiv:2205.13504*, 2022.
- [51] H. Zhao, R. T. Des Combes, K. Zhang, and G. Gordon. On learning invariant representations for domain adaptation. In *International Conference on Machine Learning*, pages 7523–7532. PMLR, 2019.
- [52] S. Zhao, M. Gong, T. Liu, H. Fu, and D. Tao. Domain generalization via entropy regularization. *Advances in Neural Information Processing Systems*, 33:16096–16107, 2020.
- [53] H. Zhou, S. Zhang, J. Peng, S. Zhang, J. Li, H. Xiong, and W. Zhang. Informer: Beyond efficient transformer for long sequence time-series forecasting. In *Proceedings of the AAAI Conference on Artificial Intelligence*, volume 35, pages 11106–11115, 2021.
- [54] T. Zhou, Z. Ma, Q. Wen, X. Wang, L. Sun, and R. Jin. Fedformer: Frequency enhanced decomposed transformer for long-term series forecasting. In *International Conference on Machine Learning*, pages 27268–27286. PMLR, 2022.

## Supplementary Material.

### A Details on the doubly residual stacking architecture in Sections 3.2 and 4.1

The  $m$ -th residual operators  $(\psi^m, \xi_{\downarrow}^m, \xi_{\uparrow}^m) \in \Psi \times \Xi_{\downarrow} \times \Xi_{\uparrow}$ ,  $m = 1, \dots, M$ , are given by

$$\begin{aligned}\psi^m(x) &:= (\text{FC}^{m,N} \circ \text{FC}^{m,N-1} \dots \circ \text{FC}^{m,1})(x), & x \in \mathcal{X} = \mathbb{R}^{\alpha}, \\ \xi_{\downarrow}^m(z) &:= \mathbf{V}_{m,\downarrow} \mathbf{W}_{m,\downarrow} z, & z \in \mathcal{Z} = \mathbb{R}^{\gamma}, \\ \xi_{\uparrow}^m(z) &:= \mathbf{V}_{m,\uparrow} \mathbf{W}_{m,\uparrow} z, & z \in \mathcal{Z} = \mathbb{R}^{\gamma}.\end{aligned}\tag{A.1}$$

These operators correspond to the  $m$ -th stack and involve fully connected layers denoted by  $\text{FC}^{m,n}$  with  $\text{ReLU}$  activation function [32]. Specifically,  $\text{FC}^{m,n}(x)$  is defined as  $\text{ReLU}(\mathbf{W}_{m,n}x + \mathbf{b}_{m,n})$ , where  $\mathbf{W}_{m,n}$  and  $\mathbf{b}_{m,n}$  are trainable weight and bias parameters, respectively. The matrix  $\mathbf{W}_{m,\downarrow} \in \mathbb{R}^{\gamma_{\downarrow} \times \gamma}$  (resp.  $\mathbf{W}_{m,\uparrow} \in \mathbb{R}^{\gamma_{\uparrow} \times \gamma}$ ) represents a trainable linear projection layer for forecasting (resp. backcasting) operations. For the parameters  $\beta$ ,  $\alpha$ , and  $\gamma$  denoting to the forecast horizon, lookback horizon, and latent space dimension, respectively (defined in Section 3),  $\mathbf{V}_{m,\downarrow} \in \mathbb{R}^{\beta \times \gamma_{\downarrow}}$  (resp.  $\mathbf{V}_{m,\uparrow} \in \mathbb{R}^{\alpha \times \gamma_{\uparrow}}$ ) represents a forecast basis (resp. backcast basis) matrix, given by

$$\begin{aligned}\mathbf{V}_{m,\downarrow} &:= (\mathbf{v}_{m,\downarrow}^1, \dots, \mathbf{v}_{m,\downarrow}^{\gamma_{\downarrow}}) \in \mathbb{R}^{\beta \times \gamma_{\downarrow}} \quad \text{with} \quad \mathbf{v}_{m,\downarrow}^1, \dots, \mathbf{v}_{m,\downarrow}^{\gamma_{\downarrow}} \in \mathbb{R}^{\beta}, \\ (\text{resp. } \mathbf{V}_{m,\uparrow} &:= (\mathbf{v}_{m,\uparrow}^1, \dots, \mathbf{v}_{m,\uparrow}^{\gamma_{\uparrow}}) \in \mathbb{R}^{\alpha \times \gamma_{\uparrow}} \quad \text{with} \quad (\mathbf{v}_{m,\uparrow}^1, \dots, \mathbf{v}_{m,\uparrow}^{\gamma_{\uparrow}}) \in \mathbb{R}^{\alpha}),\end{aligned}\tag{A.2}$$

and each  $\mathbf{v}_{m,\downarrow}^i$  (resp.  $\mathbf{v}_{m,\uparrow}^i$ ), is a forecast basis (resp. backcast basis) vector.

Note that  $\mathbf{V}_{m,\downarrow}$  and  $\mathbf{V}_{m,\uparrow}$  are set to be non-trainable parameter sets that embrace vital information for time series forecasting purposes, including trends and seasonality. These parameter sets are based on [34]. The basis expansion representations in (A.1) with flexible adjustments in (A.2) allow the model to capture the relevant patterns in the sequential data.

The main difference between N-BEATS-G and N-BEATS-I lies on the utilization of  $\mathbf{V}_{m,\downarrow}$  and  $\mathbf{V}_{m,\uparrow}$ . More precisely, N-BEATS-G does not incorporate any specialized time series-specific knowledge and instead employs the identity matrices for  $\mathbf{V}_{m,\downarrow}$  and  $\mathbf{V}_{m,\uparrow}$ . In contrast, N-BEATS-I captures trend and seasonality information, which derive the interpretability. Specifically,  $\mathbf{V}_{m,\downarrow}$  is given by  $\mathbf{V}_{m,\downarrow} = (\mathbf{1}, \mathbf{t}, \dots, \mathbf{t}^{\gamma_{\downarrow}})$ , where  $\mathbf{t} = \frac{1}{\beta}(0, 1, 2, \dots, \beta - 2, \beta - 1)^{\top}$ . This choice is motivated by the characteristic of trends, which are typically represented by monotonic or slowly varying functions. For the seasonality,  $\mathbf{V}_{m,\downarrow}$  is defined using a periodic function, (specifically the Fourier series), so that  $\mathbf{V}_{m,\downarrow} = (\mathbf{1}, \cos(2\pi\mathbf{t}), \dots, \cos(2\pi\lfloor\beta/2 - 1\rfloor\mathbf{t}), \sin(2\pi\mathbf{t}), \dots, \sin(2\pi\lfloor\beta/2 - 1\rfloor\mathbf{t}))^{\top}$ . The dimension of  $\mathbf{V}_{m,\downarrow}$  is determined by adjusting the interval between  $\cos(2\pi\mathbf{t})$  and  $\cos(2\pi\lfloor\beta/2 - 1\rfloor\mathbf{t})$ , as well as  $\sin(2\pi\mathbf{t})$  and  $\sin(2\pi\lfloor\beta/2 - 1\rfloor\mathbf{t})$ . This formulation incorporates the notion of sinusoidal waveforms to capture the periodic nature of seasonality. The formulation of  $\mathbf{V}_{m,\uparrow}$  is identical to that of  $\mathbf{V}_{m,\downarrow}$ , with the only difference being the replacement of  $\alpha$  with  $\beta$  and  $\gamma_{\downarrow}$  with  $\gamma_{\uparrow}$ .

Since each  $\psi^m$ , as defined in (A.1), is an  $N$ -layered fully connected network with the 1-Lipschitz continuous activation, i.e.,  $\text{ReLU}$ , we can apply [43, Section 6] to have an explicit representation for the (Rademacher) Lipschitz constant  $C_m > 0$  of  $\psi^m$  [10, Theorem 3.1.6]. Furthermore, the forecasting and backcasting operators,  $\xi_{\downarrow}^m$  and  $\xi_{\uparrow}^m$ , are matrix operators, and we can calculate their Lipschitz constants  $C_{m,\downarrow}$  and  $C_{m,\uparrow}$  by using the matrix norm induced by the Euclidean norm  $\|\cdot\|$ , i.e.,  $C_{m,\downarrow} := \|\mathbf{V}_{m,\downarrow} \mathbf{W}_{m,\downarrow}\| > 0$  and  $C_{m,\uparrow} := \|\mathbf{V}_{m,\uparrow} \mathbf{W}_{m,\uparrow}\| > 0$ .

*Proof of Lemma 4.1.* From the definition of  $\sigma \circ g^m$  in Definition 4.1 and the Lipschitz continuity of  $\sigma$  and  $\psi^m$  with corresponding constants  $C_{\sigma} > 0$  and  $C_m > 0$ , it follows for every  $m = 1, \dots, M$ , that for any  $x, y \in \mathcal{X}$ ,

$$\begin{aligned}\|\sigma \circ g^m(x) - \sigma \circ g^m(y)\| &\leq C_{\sigma} \|g^m(x) - g^m(y)\| \\ &\leq C_{\sigma} C_m \left\| \left( (r^m)^{(L-1)} \circ (r^{m-1})^{(L)} \circ \dots \circ (r^1)^{(L)} \right)(x) \right. \\ &\quad \left. - \left( (r^m)^{(L-1)} \circ (r^{m-1})^{(L)} \circ \dots \circ (r^1)^{(L)} \right)(y) \right\|.\end{aligned}\tag{A.3}$$

Based on the residual operation in (6) (in Definition 4.1), i.e.,  $r^m(x) = x - (\xi_{\uparrow}^m \circ \psi^m)(x)$ , and considering the Lipschitz continuity of  $\sigma$  and  $\psi^m$  with respective constants  $C_{\sigma} > 0$  and  $C_m > 0$ , we

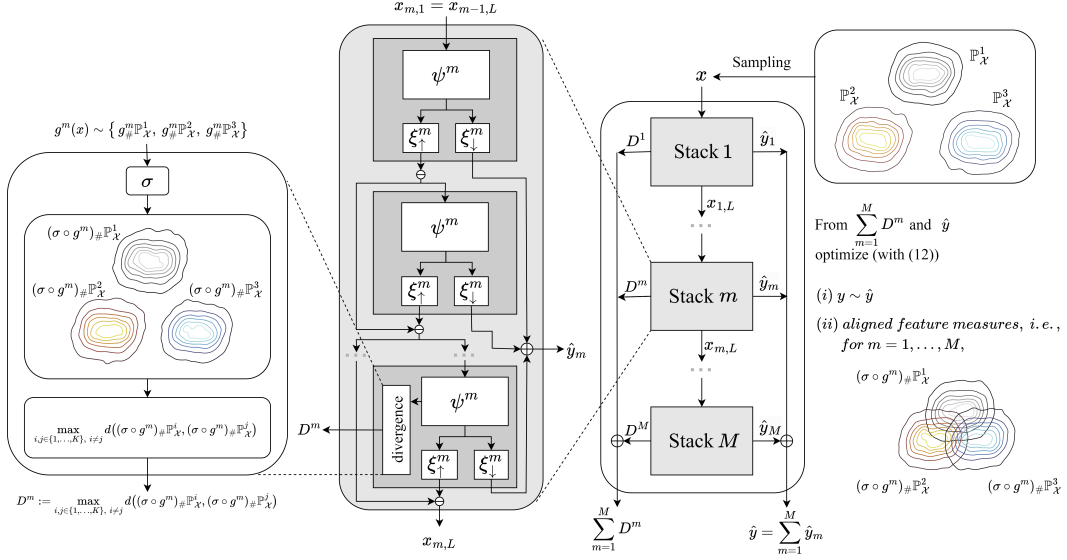


Figure 2: A schematic illustration of Feature-aligned N-BEATS.

can establish the following inequality for every  $m = 1, \dots, M$ , and any  $x, y \in \mathcal{X}$ ,

$$\|r^m(x) - r^m(y)\| \leq \|x - y\| + \|(\xi_{\uparrow}^m \circ \psi^m)(x) - (\xi_{\uparrow}^m \circ \psi^m)(y)\| \leq (1 + C_{m,\uparrow} C_m) \|x - y\|.$$

Applying this to  $L - 1$ -times composition of  $r^m$ , i.e.,  $(r^m)^{(L-1)}$ , we have  $\|(r^m)^{(L-1)}(x) - (r^m)^{(L-1)}(y)\| \leq (1 + C_{m,\uparrow} C_m)^{L-1} \|x - y\|$  for any  $x, y \in \mathcal{X}$ . Using the same arguments for the remaining compositions  $(r^{m-1})^{(L)}$ ,  $(r^{m-2})^{(L)}$ ,  $\dots$ ,  $(r^1)^{(L)}$  in (A.3), we deduce that for any  $x, y \in \mathcal{X}$ ,

$$\|\sigma \circ g^m(x) - \sigma \circ g^m(y)\| \leq C_{\sigma} C_m (1 + C_m C_{m,\uparrow})^{L-1} \prod_{n=1}^{m-1} (1 + C_n C_{n,\uparrow})^L \|x - y\| = C_{\sigma \circ g^m} \|x - y\|.$$

This completes the proof.  $\square$

## B Specifics on the regularized Wasserstein distances in Section 4.2

*Proof of Theorem 4.1.* From the dual representation in [37, Remark 4.18 in Section 4.4] based on the Lagrangian method and the integral property of pushforward measures in [2, Section 5.2], it follows for every  $m = 1, \dots, M$  that given  $\mathbb{P}_{\mathcal{X}}^i, \mathbb{P}_{\mathcal{X}}^j \in \{\mathbb{P}_{\mathcal{X}}^k\}_{k=1}^K$  with  $i \neq j$ ,

$$\begin{aligned} & \mathcal{W}_{\epsilon, \tilde{\mathcal{Z}}}((\sigma \circ g^m)_{\#} \mathbb{P}_{\mathcal{X}}^i, (\sigma \circ g^m)_{\#} \mathbb{P}_{\mathcal{X}}^j) \\ &= \sup_{\tilde{f}, \tilde{h} \in \mathcal{C}(\tilde{\mathcal{Z}})} \left\{ \int_{\tilde{\mathcal{Z}}} \tilde{f}(x) d((\sigma \circ g^m)_{\#} \mathbb{P}_{\mathcal{X}}^i)(x) + \int_{\tilde{\mathcal{Z}}} \tilde{h}(y) d((\sigma \circ g^m)_{\#} \mathbb{P}_{\mathcal{X}}^j)(y) \right. \\ & \quad \left. - \epsilon \int_{\tilde{\mathcal{Z}} \times \tilde{\mathcal{Z}}} e^{\frac{1}{\epsilon}(\tilde{f}(x) + \tilde{h}(y) - \|x - y\|^2)} d((\sigma \circ g^m)_{\#} \mathbb{P}_{\mathcal{X}}^i) \otimes ((\sigma \circ g^m)_{\#} \mathbb{P}_{\mathcal{X}}^j)(x, y) \right\} \quad (\text{B.1}) \\ &= \sup_{f, h \in \mathcal{C}(\mathcal{X}; \sigma \circ g^m)} \left\{ \int_{\mathcal{X}} f(x) d\mathbb{P}_{\mathcal{X}}^i(x) + \int_{\mathcal{X}} h(y) d\mathbb{P}_{\mathcal{X}}^j(y) \right. \\ & \quad \left. - \epsilon \int_{\mathcal{X} \times \mathcal{X}} e^{\frac{1}{\epsilon}(f(x) + h(y) - \|(\sigma \circ g^m)(x) - (\sigma \circ g^m)(y)\|^2)} d(\mathbb{P}_{\mathcal{X}}^i \otimes \mathbb{P}_{\mathcal{X}}^j)(x, y) \right\}, \end{aligned}$$

where  $\mathcal{C}(\tilde{\mathcal{Z}})$  denotes the set of all real-valued continuous functions on  $\tilde{\mathcal{Z}}$  and  $\mathcal{C}(\mathcal{X}; \sigma \circ g^m)$  is given by  $\mathcal{C}(\mathcal{X}; \sigma \circ g^m) := \{f : \mathcal{X} \rightarrow \mathbb{R} \mid \exists \tilde{f} \in \mathcal{C}(\tilde{\mathcal{Z}}) \text{ s.t. } f = \tilde{f} \circ \sigma \circ g^m\}$ .

Consider the following regularized optimal transport problem:

$$\begin{aligned} \widehat{\mathcal{W}}_{\epsilon, \mathcal{X}}(\mathbb{P}^i, \mathbb{P}^j; \sigma \circ g^m) := & \inf_{\pi \in \Pi(\mathbb{P}^i, \mathbb{P}^j; \mathcal{X})} \left\{ \int_{\mathcal{X} \times \mathcal{X}} (\|\sigma \circ g^m(x) - \sigma \circ g^m(y)\|^2 \right. \\ & \left. + \epsilon \log \left( \frac{d\pi(x, y)}{d\mathbb{P}_{\mathcal{X}}^i(x) d\mathbb{P}_{\mathcal{X}}^j(y)} \right) \right\} d\pi(x, y). \end{aligned}$$

Then, from the dual representation, as in (B.1), it follows that

$$\begin{aligned} \widehat{\mathcal{W}}_{\epsilon, \mathcal{X}}(\mathbb{P}^i, \mathbb{P}^j; \sigma \circ g^m) = & \sup_{f, h \in \mathcal{C}(\mathcal{X})} \left\{ \int_{\mathcal{X}} f(x) d\mathbb{P}_{\mathcal{X}}^i(x) + \int_{\mathcal{X}} h(y) d\mathbb{P}_{\mathcal{X}}^j(y) \right. \\ & \left. - \epsilon \int_{\mathcal{X} \times \mathcal{X}} e^{\frac{1}{\epsilon}(f(x)+h(y)-\|(\sigma \circ g^m)(x)-(\sigma \circ g^m)(y)\|^2)} d(\mathbb{P}_{\mathcal{X}}^i \otimes \mathbb{P}_{\mathcal{X}}^j)(x, y) \right\}, \end{aligned} \quad (\text{B.2})$$

where  $\mathcal{C}(\mathcal{X})$  denotes the set of all continuous real-valued functions on  $\mathcal{X}$ . From the dual representations in (B.1) and (B.2) and the relation that  $\mathcal{C}(\mathcal{X}; \sigma \circ g^m) \subseteq \mathcal{C}(\mathcal{X})$ , it follows that

$$\mathcal{W}_{\epsilon, \tilde{\mathcal{Z}}}((\sigma \circ g^m)_{\#} \mathbb{P}_{\mathcal{X}}^i, (\sigma \circ g^m)_{\#} \mathbb{P}_{\mathcal{X}}^j) \leq \widehat{\mathcal{W}}_{\epsilon, \mathcal{X}}(\mathbb{P}^i, \mathbb{P}^j; \sigma \circ g^m). \quad (\text{B.3})$$

On the other hand, from the first order optimality condition and the continuity of  $\sigma \circ g^m$  (see Lemma 4.1), it follows that the optimal potentials  $f^*, h^* \in \mathcal{C}(\mathcal{X})$ , which realize the supremum (B.2), are given by, respectively,

$$\begin{aligned} f^*(x) &:= -\epsilon \log \left( \int_{\mathcal{X}} e^{\frac{1}{\epsilon}(h^*(y)-\|(\sigma \circ g^m)(x)-(\sigma \circ g^m)(y)\|^2)} d\mathbb{P}_{\mathcal{X}}^j(y) \right), \quad x \in \mathcal{X}, \\ h^*(y) &:= -\epsilon \log \left( \int_{\mathcal{X}} e^{\frac{1}{\epsilon}(f^*(x)-\|(\sigma \circ g^m)(x)-(\sigma \circ g^m)(y)\|^2)} d\mathbb{P}_{\mathcal{X}}^i(x) \right), \quad y \in \mathcal{X}, \end{aligned} \quad (\text{B.4})$$

which can be represented by  $f^* = \tilde{f}^* \circ \sigma \circ g^m$  and  $h^* = \tilde{h}^* \circ \sigma \circ g^m$ , respectively, where  $\tilde{f}^*, \tilde{h}^* \in \mathcal{C}(\tilde{\mathcal{Z}})$  are given by, respectively,

$$\begin{aligned} \tilde{f}^*(x) &:= -\epsilon \log \left( \int_{\mathcal{X}} e^{\frac{1}{\epsilon}(\tilde{h}^* \circ \sigma \circ g^m)(y) - \|x - (\sigma \circ g^m)(y)\|^2} d\mathbb{P}_{\mathcal{X}}^j(y) \right), \quad x \in \tilde{\mathcal{Z}}, \\ \tilde{h}^*(y) &:= -\epsilon \log \left( \int_{\mathcal{X}} e^{\frac{1}{\epsilon}(\tilde{f}^* \circ \sigma \circ g^m)(x) - \|(\sigma \circ g^m)(x) - y\|^2} d\mathbb{P}_{\mathcal{X}}^i(x) \right), \quad y \in \tilde{\mathcal{Z}}. \end{aligned} \quad (\text{B.5})$$

This ensures that  $f^*, h^* \in \mathcal{C}(\mathcal{X}; \sigma \circ g^m) \subseteq \tilde{\mathcal{C}}(\mathcal{X})$ . Hence we establish that (B.3) holds as equality.

From this and the Lipschitz continuity of  $\sigma \circ g^m$  with the constant  $C_{\sigma \circ g^m} > 0$  in Lemma 4.1., it follows that

$$\begin{aligned} \mathcal{W}_{\epsilon, \tilde{\mathcal{Z}}}((\sigma \circ g^m)_{\#} \mathbb{P}_{\mathcal{X}}^i, (\sigma \circ g^m)_{\#} \mathbb{P}_{\mathcal{X}}^j) &= \widehat{\mathcal{W}}_{\epsilon, \mathcal{X}}(\mathbb{P}^i, \mathbb{P}^j; \sigma \circ g^m) \\ &\leq \inf_{\pi \in \Pi(\mathbb{P}^i, \mathbb{P}^j; \mathcal{X})} \left\{ \int_{\mathcal{X} \times \mathcal{X}} \left( C_{\sigma \circ g^m}^2 \|x - y\|^2 + \epsilon \log \left( \frac{d\pi(x, y)}{d\mathbb{P}_{\mathcal{X}}^i(x) d\mathbb{P}_{\mathcal{X}}^j(y)} \right) \right) d\pi(x, y) \right\} \\ &\leq \max\{C_{\sigma \circ g^m}^2, 1\} \mathcal{W}_{\epsilon, \mathcal{X}}(\mathbb{P}^i, \mathbb{P}^j). \end{aligned} \quad (\text{B.6})$$

Therefore, we conclude that

$$\begin{aligned} & \sum_{m=1}^M \max_{i, j \in \{1, \dots, K\}, i \neq j} \mathcal{W}_{\epsilon, \tilde{\mathcal{Z}}}((\sigma \circ g^m)_{\#} \mathbb{P}_{\mathcal{X}}^i, (\sigma \circ g^m)_{\#} \mathbb{P}_{\mathcal{X}}^j) \\ & \leq \sum_{m=1}^M \max\{C_{\sigma \circ g^m}^2, 1\} \max_{i, j \in \{1, \dots, K\}, i \neq j} \mathcal{W}_{\epsilon, \mathcal{X}}(\mathbb{P}^i, \mathbb{P}^j) = C \max_{i, j \in \{1, \dots, K\}, i \neq j} \mathcal{W}_{\epsilon, \mathcal{X}}(\mathbb{P}^i, \mathbb{P}^j), \end{aligned}$$

with  $C = \sum_{m=1}^M \max\{C_{\sigma \circ g^m}^2, 1\}$ . This completes the proof.  $\square$

From the nonnegativity of the entropy term in the regularized Wasserstein distance  $\mathcal{W}_{\epsilon, \tilde{\mathcal{Z}}}$ , i.e.,

$$\int_{\tilde{\mathcal{Z}} \times \tilde{\mathcal{Z}}} \epsilon \log \left( \frac{d\pi(x, y)}{d\mu(x)d\nu(y)} \right) d\pi(x, y) \geq 0, \quad \forall \pi \in \Pi(\mu, \nu; \tilde{\mathcal{Z}}),$$

it is clear that  $\mathcal{W}_{\epsilon, \tilde{\mathcal{Z}}}(\mu, \nu) \geq 0 \forall \mu, \nu \in \mathcal{P}(\tilde{\mathcal{Z}})$ . Moreover, from the definition of Sinkhorn divergence  $\widehat{\mathcal{W}}_{\epsilon, \tilde{\mathcal{Z}}}$ , i.e.,  $\widehat{\mathcal{W}}_{\epsilon, \tilde{\mathcal{Z}}}(\mu, \nu) = \mathcal{W}_{\epsilon, \tilde{\mathcal{Z}}}(\mu, \nu) - \frac{1}{2}(\mathcal{W}_{\epsilon, \tilde{\mathcal{Z}}}(\nu, \nu) + \mathcal{W}_{\epsilon, \tilde{\mathcal{Z}}}(\mu, \mu))$ ,  $\forall \mu, \nu \in \mathcal{P}(\tilde{\mathcal{Z}})$ , it follows that the Sinkhorn divergence  $\widehat{\mathcal{W}}_{\epsilon, \tilde{\mathcal{Z}}}$  and the regularized quadratic Wasserstein distance  $\mathcal{W}_{\epsilon, \tilde{\mathcal{Z}}}$  satisfy

$$\widehat{\mathcal{W}}_{\epsilon, \tilde{\mathcal{Z}}}(\mu, \nu) \leq \mathcal{W}_{\epsilon, \tilde{\mathcal{Z}}}(\mu, \nu), \quad \forall \mu, \nu \in \mathcal{P}(\tilde{\mathcal{Z}}).$$

Hence, using Theorem 4.1, we immediately obtain the following result of the representation learning bound under the Sinkhorn divergence  $\widehat{\mathcal{W}}_{\epsilon, \tilde{\mathcal{Z}}}$  by using the the pair-wise divergence of source domains' measures under regularized quadratic Wasserstein distance  $\mathcal{W}_{\epsilon, \mathcal{X}}$ .

**Corollary B.1.** *For any  $\epsilon \geq 0$ , the following holds*

$$\sum_{m=1}^M \max_{i, j \in \{1, \dots, K\}, i \neq j} \widehat{\mathcal{W}}_{\epsilon, \tilde{\mathcal{Z}}}((\sigma \circ g^m)_{\#} \mathbb{P}_{\mathcal{X}}^i, (\sigma \circ g^m)_{\#} \mathbb{P}_{\mathcal{X}}^j) \leq C \max_{i, j \in \{1, \dots, K\}, i \neq j} \mathcal{W}_{\epsilon, \mathcal{X}}(\mathbb{P}_{\mathcal{X}}^i, \mathbb{P}_{\mathcal{X}}^j),$$

with  $C = \sum_{m=1}^M \max\{(C_{\sigma \circ g^m})^2, 1\} > 0$  (defined in Theorem 4.1).

## C Experimental Environment

- CPU: Intel(R) Xeon(R) Platinum 8163 CPU @ 2.50GHz
- GPU: NVIDIA TITAN RTX

All the experiments are performed within the aforementioned environments. Moreover, the subsequent analysis presented in Section E is likewise carried out within the same environment. A more comprehensive software environment is available on GitHub (It will be disclosed upon acceptance).

## D Experimental Details in Section 5

### D.1 Dataset Configuration

Real-world financial and weather data are collected from reputable sources, namely the Federal Reserve Bank of St. Louis (FRED)<sup>5</sup> and the National Oceanic and Atmospheric Administration (NOAA)<sup>6</sup>, as mentioned in the main paper. The procedure for generating training data is as follows.

1. Crawl finance data {commodity, income, interest rate, exchange rate} from FRED and weather data {pressure, rain, temperature, wind} from NOAA.
2. Segment each data point into a sliding window of a specified size [lookback, forecast] (e.g., [50, 10]), where the sliding stride is set to 1, and subsequently designate each segment as an individual instance.
3. To alleviate any potential concerns arising from data imbalance, we establish a predetermined quantity of 7,500 instances for each domain through the utilization of random sampling techniques, thereby guaranteeing independence from such considerations.

Note that to alleviate the complexity of our evaluation scenario, we refrain from altering the frequency of each data instance during the collection process. The graphical representation of the frequency distribution for instances is depicted in Figure 3.

### D.2 Hyperparameter

Considering the scope of our experimental configuration that bring a total of 184 experimental cases for each model, we adopt a suitable range of hyperparameters to achieve the performance results presented in Table 1 of the main paper. The details are provided in Table 2.

<sup>5</sup><https://fred.stlouisfed.org>

<sup>6</sup><https://ncei.noaa.gov>

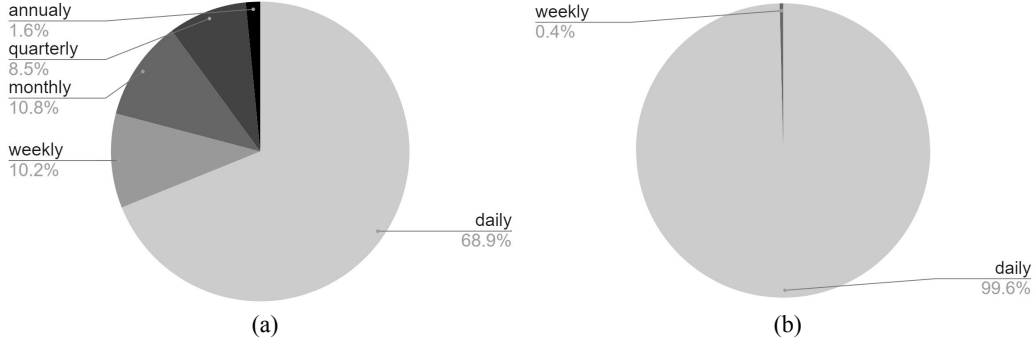


Figure 3: **Graphical representation of the frequency distribution.** (a) FRED, and (b) NOAA.

Table 2: **Hyperparameters.**

HYPERPARAMETER	CONSIDERED VALUES
Lookback horizon.	$\alpha = 50$
Forecast horizon.	$\beta = 10$
Number of stacks.	$M = 3$
Number of blocks in each stack.	$L = 4$
Activation function.	ReLU
Feature dimension.	$\gamma = 512$
Loss function.	$\mathcal{L} = \text{sMAPE}$
Regularizing temperature.	$\lambda \in \{0.1, 0.3, 1, 3\}$
Learning rate scheduling.	CyclicLR(base lr=2e-7, max lr=2e-5, mode="triangular2", step_size_up=10)
Batch size.	$B = 2^{12}$
Number of iterations.	1,000
Type of stacks used for N-BEATS-I.	[Trend, Seasonality, Seasonality] [34]
Number of polynomials and harmonics used for N-BEATS-I.	2
Pooling method used for N-HiTS.	MaxPool1d
Interpolation method used for N-HiTS.	interpolate(mode="linear")
Kernel size used for N-HiTS.	2

### D.3 Evaluation Metrics

We adopt the following two evaluation metrics: given  $H = N \times \beta$  with  $N$  denoting the number of instances,

$$\text{sMAPE} = \frac{2}{H} \sum_{i=1}^H \frac{|y_i - \hat{y}_i|}{|y_i| + |\hat{y}_i|}, \quad \text{MASE} = \frac{\frac{1}{H} \sum_{i=1}^H |y_i - \hat{y}_i|}{\frac{1}{H-1} \sum_{i=1}^{H-1} |y_{i+1} - y_i|}.$$

## E Further Analysis

### E.1 Stack-wise alignment vs Block-wise alignment

We provide a performance comparison between the stack-wise and block-wise feature alignments and the results are given in Table 3. While the stack-wise alignment generally exhibits better performance for N-HiTS and N-BEATS-G cases, the block-wise alignment performs better for N-BEATS-I case. In contrast to N-BEATS-G, where the FC-layers' outputs are immediately employed for forecasting (due to the identity matrices  $\mathbf{V}_{m,\downarrow}$  and  $\mathbf{V}_{m,\uparrow}$ , see Section A), N-BEATS-I's outputs are linear combinations of (non-trainable) interpretable basis  $\mathbf{V}_{m,\downarrow}$  and  $\mathbf{V}_{m,\uparrow}$ , where the coefficients of the combinations are determined by FC-layers' outputs. We speculate that due to the influence of relatively fewer trainable parameters in N-BEATS-I (compared to N-BEATS-G), the model suffers less from gradient-related issues arising from the alignment. Thus, this advantage of N-BEATS-I allows it to align the feature measures in every block of the stacking architecture. It is worth noting that while the outcomes in N-BEATS-I are not consistent with the results in N-BEATS-G and N-HiTS cases, both the block-wise and stack-wise alignment in N-BEATS-I still outperforms vanilla N-BEATS-I.

Table 3: **Comparative analysis between stack-wise and block-wise alignment.** We adhere precisely to the identical experimental configuration presented in Table 1 of the main paper. B-FA and S-FA denote block-wise and stack-wise feature alignment, respectively.

Baseline		N-HiTS				N-BEATS-I				N-BEATS-G			
Method		+ B-FA		S-FA (ours)		+ B-FA		S-FA (ours)		+ B-FA		S-FA (ours)	
Metric		SMAPE	MASE	SMAPE	MASE	SMAPE	MASE	SMAPE	MASE	SMAPE	MASE	SMAPE	MASE
<i>In-domain Generalization</i>													
FRED	Commodity	0.081	0.045	<b>0.068</b>	<b>0.043</b>	<b>0.075</b>	<b>0.044</b>	0.126	0.053	<b>0.074</b>	0.044	0.080	0.044
	Income	0.302	0.056	<b>0.297</b>	<b>0.054</b>	<b>0.301</b>	0.056	0.302	<b>0.055</b>	0.302	0.056	<b>0.298</b>	<b>0.055</b>
	Interest rate	0.079	0.083	<b>0.071</b>	<b>0.081</b>	<b>0.079</b>	<b>0.082</b>	0.086	0.091	0.079	0.083	<b>0.074</b>	<b>0.081</b>
	Exchange rate	0.025	0.051	<b>0.024</b>	<b>0.050</b>	<b>0.025</b>	<b>0.051</b>	0.029	0.056	0.025	0.051	<b>0.024</b>	<b>0.050</b>
NOAA	Pressure	0.384	0.276	0.384	<b>0.272</b>	<b>0.383</b>	0.277	0.389	<b>0.263</b>	0.384	0.276	0.384	0.276
	Rain	1.818	1.681	<b>1.776</b>	<b>1.208</b>	<b>1.798</b>	<b>1.535</b>	1.805	3.046	1.817	1.676	<b>1.776</b>	<b>1.208</b>
	Temperature	0.247	0.243	0.247	<b>0.242</b>	0.245	0.242	<b>0.231</b>	<b>0.227</b>	0.246	0.243	<b>0.245</b>	<b>0.241</b>
	Wind	0.453	0.641	<b>0.452</b>	<b>0.640</b>	0.453	0.641	<b>0.434</b>	<b>0.623</b>	0.453	0.641	<b>0.452</b>	<b>0.640</b>
Average		0.424	0.384	<b>0.415</b>	<b>0.324</b>	<b>0.420</b>	<b>0.366</b>	0.424	0.551	0.423	0.384	<b>0.417</b>	<b>0.325</b>
<i>Cross-domain Generalization</i>													
FRED	Commodity	0.102	0.046	<b>0.081</b>	<b>0.044</b>	<b>0.105</b>	<b>0.046</b>	0.197	0.059	0.108	0.047	<b>0.107</b>	<b>0.046</b>
	Income	0.301	0.054	<b>0.295</b>	<b>0.053</b>	<b>0.301</b>	<b>0.055</b>	0.323	0.070	0.301	0.054	<b>0.295</b>	<b>0.053</b>
	Interest rate	0.099	0.076	<b>0.085</b>	<b>0.074</b>	<b>0.097</b>	0.076	0.146	<b>0.054</b>	0.101	0.078	<b>0.100</b>	<b>0.077</b>
	Exchange rate	0.031	0.056	<b>0.029</b>	<b>0.055</b>	<b>0.031</b>	0.098	0.055	<b>0.063</b>	0.032	0.055	<b>0.031</b>	0.055
NOAA	Pressure	<b>0.371</b>	0.263	0.372	<b>0.260</b>	<b>0.370</b>	<b>0.262</b>	0.405	0.299	0.373	0.264	<b>0.372</b>	<b>0.263</b>
	Rain	1.809	1.144	<b>1.803</b>	<b>0.783</b>	1.808	<b>1.148</b>	<b>1.787</b>	1.831	1.804	1.181	1.804	<b>1.178</b>
	Temperature	0.246	0.244	<b>0.245</b>	<b>0.242</b>	0.246	0.244	<b>0.240</b>	0.244	0.246	0.244	<b>0.245</b>	<b>0.243</b>
	Wind	0.453	0.644	<b>0.452</b>	<b>0.643</b>	0.454	<b>0.644</b>	<b>0.439</b>	0.646	0.453	0.643	<b>0.452</b>	0.643
Average		0.427	0.316	<b>0.420</b>	<b>0.269</b>	<b>0.426</b>	<b>0.322</b>	0.449	0.408	0.427	0.321	<b>0.426</b>	<b>0.319</b>
<i>Out-domain Generalization</i>													
FRED	Commodity	0.137	0.049	<b>0.103</b>	<b>0.046</b>	<b>0.133</b>	<b>0.049</b>	0.258	0.069	0.137	0.049	<b>0.136</b>	0.049
	Income	0.306	0.056	<b>0.298</b>	<b>0.055</b>	<b>0.305</b>	<b>0.055</b>	0.335	0.075	0.306	0.056	<b>0.304</b>	<b>0.055</b>
	Interest rate	0.121	0.074	<b>0.100</b>	<b>0.070</b>	<b>0.119</b>	0.073	0.189	<b>0.046</b>	0.121	0.075	<b>0.120</b>	<b>0.073</b>
	Exchange rate	0.040	0.060	<b>0.034</b>	<b>0.058</b>	<b>0.040</b>	<b>0.060</b>	0.075	0.069	0.040	0.060	<b>0.039</b>	0.060
NOAA	Pressure	0.368	0.255	<b>0.350</b>	<b>0.250</b>	<b>0.367</b>	<b>0.254</b>	0.409	0.305	0.368	0.255	<b>0.367</b>	0.255
	Rain	1.806	1.094	<b>1.804</b>	<b>0.910</b>	1.806	<b>1.094</b>	<b>1.793</b>	1.430	1.807	1.091	<b>1.806</b>	<b>0.918</b>
	Temperature	0.247	0.245	<b>0.245</b>	<b>0.243</b>	0.247	0.245	<b>0.246</b>	0.255	0.247	0.245	<b>0.246</b>	<b>0.244</b>
	Wind	0.456	0.645	<b>0.454</b>	<b>0.644</b>	0.456	<b>0.645</b>	<b>0.449</b>	0.662	0.457	0.645	<b>0.454</b>	0.645
Average		0.435	0.310	<b>0.424</b>	<b>0.182</b>	<b>0.434</b>	<b>0.309</b>	0.469	0.364	0.435	0.309	<b>0.433</b>	<b>0.287</b>

## E.2 Other metrics for feature alignment

We provide another performance comparison with other metrics for stack-wise alignment. The following metrics are commonly used for the representation learning framework:

(i) The Kullback-Leibler (KL) divergence: for every  $\mu, \nu \in \mathcal{P}(\tilde{\mathcal{Z}})$ ,

$$\text{KL}(\mu \parallel \nu) = \int_{\tilde{\mathcal{Z}}} \log \left( \frac{\mu(dz)}{\nu(dz)} \right) \mu(dz);$$

(ii) The maximum mean discrepancy (MMD): for every  $\mu, \nu \in \mathcal{P}(\tilde{\mathcal{Z}})$ ,

$$\text{MMD}_{\mathcal{F}}(\mu, \nu) = \sup_{f \in \mathcal{F}} \left( \int_{\tilde{\mathcal{Z}}} f(x) \mu(dx) - \int_{\tilde{\mathcal{Z}}} f(y) \nu(dy) \right),$$

where  $\mathcal{F}$  denotes a class of functions  $f : \tilde{\mathcal{Z}} \rightarrow \mathbb{R}$  and it can be specified as the unit ball in a reproducing kernel Hilbert space. For detailed description and other possible function classes, please refer to [17, Sections 2.2, 7.1, and 7.2].

Table 4 demonstrates that Sinkhorn divergence serves as the best metric for the stack-wise feature alignment in terms of both accuracy and stability. Although KL divergence produces competitive results in specific cases, its instability becomes evident, as observed through high estimate fluctuations and instances with blowing up estimates. This issue is also reported in [15].

## E.3 Normalizing Techniques

According to the results presented in Table 5, it is observed that Feature-aligned N-BEATS generally achieves the most significant performance when softmax function is adopted. However, in some cases, tanh function and the absence of normalization function exhibit more favorable outcomes compared to the softmax case. Regarding these cases, we speculate that although the scale is an instance-wise attribute, it can exhibit domain-dependent characteristics in some cases. Therefore,

Table 4: **Examination of metrics for the entropic regularizer.** We adhere precisely to the identical experimental configuration presented in Table 1 of the main paper.

Baseline		N-HITS						N-BEATS-I						N-BEATS-G					
Method		KL		MMD		Sinkhorn (ours)		KL		MMD		Sinkhorn (ours)		KL		MMD		Sinkhorn (ours)	
Metric		sMAPE	MASE	sMAPE	MASE	sMAPE	MASE	sMAPE	MASE	sMAPE	MASE	sMAPE	MASE	sMAPE	MASE	sMAPE	MASE	sMAPE	MASE
<i>In-domain Generalization</i>																			
FRED	Commodity	NaN	NaN	0.068	0.044	0.068	<b>0.043</b>	NaN	NaN	<b>0.122</b>	<b>0.050</b>	0.126	0.053	NaN	NaN	0.082	0.045	<b>0.080</b>	<b>0.044</b>
	Income	NaN	NaN	0.299	0.057	<b>0.297</b>	<b>0.054</b>	NaN	NaN	0.308	0.058	<b>0.302</b>	<b>0.055</b>	NaN	NaN	0.301	0.056	<b>0.298</b>	<b>0.055</b>
NOAA	Interest rate	NaN	NaN	0.072	<b>0.080</b>	<b>0.071</b>	0.081	NaN	NaN	0.098	<b>0.089</b>	<b>0.086</b>	0.091	NaN	NaN	0.074	0.082	0.074	<b>0.081</b>
	Exchange rate	NaN	NaN	0.025	0.051	<b>0.024</b>	<b>0.050</b>	NaN	NaN	0.035	<b>0.055</b>	<b>0.029</b>	0.056	0.026	<b>0.049</b>	0.025	0.051	<b>0.024</b>	0.050
NOAA	Pressure	0.403	0.286	0.403	0.286	<b>0.384</b>	<b>0.272</b>	<b>0.380</b>	0.261	0.384	<b>0.259</b>	0.389	0.263	<b>0.376</b>	<b>0.274</b>	0.378	0.275	0.384	0.276
	Rain	NaN	NaN	1.849	1.421	<b>1.776</b>	<b>1.208</b>	NaN	NaN	<b>1.792</b>	<b>2.881</b>	1.805	3.046	NaN	NaN	1.817	1.687	<b>1.776</b>	<b>1.208</b>
NOAA	Temperature	NaN	NaN	0.247	0.242	0.247	0.242	NaN	NaN	0.234	0.228	<b>0.231</b>	<b>0.227</b>	NaN	NaN	0.245	0.242	0.245	<b>0.241</b>
	Wind	NaN	NaN	0.454	0.640	<b>0.452</b>	0.640	NaN	NaN	0.435	0.624	<b>0.434</b>	<b>0.623</b>	NaN	NaN	0.452	0.641	0.452	<b>0.640</b>
Average		NaN	NaN	0.427	0.353	<b>0.415</b>	<b>0.324</b>	NaN	NaN	0.426	<b>0.531</b>	<b>0.424</b>	0.551	NaN	NaN	0.422	0.385	<b>0.417</b>	<b>0.325</b>
<i>Cross-domain Generalization</i>																			
FRED	Commodity	NaN	NaN	0.086	0.045	<b>0.081</b>	<b>0.044</b>	NaN	NaN	<b>0.187</b>	<b>0.057</b>	0.197	0.059	NaN	NaN	<b>0.104</b>	0.046	0.107	0.046
	Income	NaN	NaN	0.298	0.054	<b>0.295</b>	<b>0.053</b>	<b>0.315</b>	<b>0.064</b>	0.323	0.071	0.323	0.070	0.296	<b>0.051</b>	0.301	0.055	<b>0.295</b>	0.053
NOAA	Interest rate	NaN	NaN	0.088	0.076	<b>0.085</b>	<b>0.074</b>	<b>0.115</b>	<b>0.035</b>	0.141	0.051	0.146	0.054	<b>0.088</b>	<b>0.076</b>	0.100	0.078	0.100	<b>0.077</b>
	Exchange rate	0.030	<b>0.055</b>	<b>0.029</b>	0.056	<b>0.029</b>	<b>0.055</b>	<b>0.044</b>	0.071	0.054	0.066	0.055	<b>0.063</b>	0.031	0.057	0.031	0.057	0.031	<b>0.055</b>
NOAA	Pressure	NaN	NaN	0.377	0.262	<b>0.372</b>	<b>0.260</b>	NaN	NaN	0.405	0.316	0.405	<b>0.299</b>	NaN	NaN	<b>0.370</b>	<b>0.262</b>	0.372	0.263
	Rain	NaN	NaN	1.815	0.940	<b>1.803</b>	<b>0.783</b>	NaN	NaN	1.791	1.934	<b>1.787</b>	<b>1.831</b>	NaN	NaN	<b>1.808</b>	<b>1.108</b>	<b>1.804</b>	1.178
NOAA	Temperature	NaN	NaN	0.245	0.243	0.245	<b>0.242</b>	NaN	NaN	0.241	0.245	<b>0.240</b>	<b>0.244</b>	NaN	NaN	0.246	0.244	<b>0.245</b>	<b>0.243</b>
	Wind	NaN	NaN	0.453	0.643	<b>0.452</b>	0.643	NaN	NaN	0.440	0.646	<b>0.439</b>	0.646	NaN	NaN	0.453	0.643	<b>0.452</b>	0.643
Average		NaN	NaN	0.424	0.290	<b>0.420</b>	<b>0.269</b>	NaN	NaN	<b>0.448</b>	0.423	0.449	<b>0.408</b>	NaN	NaN	0.427	<b>0.312</b>	<b>0.426</b>	0.319
<i>Out-domain Generalization</i>																			
FRED	Commodity	<b>0.100</b>	<b>0.047</b>	0.110	<b>0.046</b>	0.103	<b>0.046</b>	<b>0.222</b>	<b>0.063</b>	0.246	0.066	0.258	0.069	<b>0.133</b>	0.050	0.137	0.050	0.136	<b>0.049</b>
	Income	<b>0.293</b>	<b>0.050</b>	0.302	0.056	0.298	0.055	<b>0.320</b>	<b>0.067</b>	0.338	0.082	0.335	0.075	<b>0.300</b>	<b>0.052</b>	0.305	0.055	0.304	0.055
NOAA	Interest rate	<b>0.100</b>	<b>0.070</b>	0.107	0.083	0.104	0.074	0.189	0.046	<b>0.165</b>	<b>0.021</b>	0.181	0.053	<b>0.120</b>	<b>0.073</b>	0.123	0.077	0.121	0.076
	Exchange rate	0.040	<b>0.053</b>	<b>0.034</b>	0.058	<b>0.034</b>	0.058	<b>0.070</b>	0.070	0.074	0.073	0.075	<b>0.069</b>	<b>0.040</b>	<b>0.057</b>	0.041	0.059	<b>0.039</b>	0.060
NOAA	Pressure	NaN	NaN	0.351	0.250	<b>0.350</b>	0.250	NaN	NaN	0.412	0.306	<b>0.409</b>	<b>0.305</b>	<b>0.365</b>	0.263	0.367	<b>0.254</b>	0.367	0.255
	Rain	NaN	NaN	1.820	0.919	<b>1.804</b>	<b>0.910</b>	NaN	NaN	1.800	1.728	<b>1.793</b>	<b>1.430</b>	1.831	0.951	1.818	1.026	<b>1.806</b>	<b>0.918</b>
NOAA	Temperature	NaN	NaN	0.246	0.244	<b>0.245</b>	<b>0.243</b>	NaN	NaN	0.248	0.255	<b>0.246</b>	0.255	0.248	0.247	0.248	0.245	<b>0.246</b>	<b>0.244</b>
	Wind	NaN	NaN	0.455	0.645	<b>0.454</b>	<b>0.644</b>	NaN	NaN	0.450	0.662	<b>0.449</b>	0.662	0.456	0.646	0.457	<b>0.645</b>	<b>0.645</b>	<b>0.644</b>
Average		NaN	NaN	0.428	0.286	<b>0.424</b>	<b>0.182</b>	NaN	NaN	0.469	0.403	0.469	<b>0.364</b>	0.437	0.293	0.437	0.301	<b>0.433</b>	<b>0.287</b>

Table 5: **Comparative study of normalizing functions.** We adhere precisely to the identical experimental configuration presented in Table 1 of the main paper.

Baseline		N-HITS						N-BEATS-I						N-BEATS-G					
Method		+ Tanh		+ Identity		+ Softmax (ours)		+ Tanh		+ Identity		+ Softmax (ours)		+ Tanh		+ Identity		+ Softmax (ours)	
Metric		sMAPE	MASE	sMAPE	MASE	sMAPE	MASE	sMAPE	MASE	sMAPE	MASE	sMAPE	MASE	sMAPE	MASE	sMAPE	MASE	sMAPE	MASE
<i>In-domain Generalization</i>																			
FRED	Commodity	0.068	0.044	0.068	0.044	0.068	<b>0.043</b>	0.142	0.055	<b>0.124</b>	<b>0.052</b>	0.126	0.053	0.083	0.045	0.083	0.045	<b>0.080</b>	<b>0.044</b>
	Income	0.299	0.058	0.299	0.057	<b>0.297</b>	<b>0.054</b>	0.308	0.058	0.310	0.059	<b>0.302</b>	<b>0.055</b>	0.302	0.057	0.302	0.056	<b>0.298</b>	<b>0.055</b>
NOAA	Interest rate	0.072	<b>0.077</b>	0.072	0.081	<b>0.071</b>	0.081	0.104	<b>0.079</b>	0.097	0.087	<b>0.086</b>	0.091	0.080	<b>0.080</b>	0.080	0.081	<b>0.074</b>	0.081
	Exchange rate	0.025	<b>0.050</b>	0.025	0.051	<b>0.024</b>	<b>0.050</b>	0.040	<b>0.055</b>	0.033	<b>0.055</b>	<b>0.029</b>	0.056	0.026	0.051	0.026	0.052	<b>0.024</b>	<b>0.050</b>
NOAA	Pressure	0.393	0.273	0.393	0.273	<b>0.384</b>	<b>0.272</b>	0.390	0.266	<b>0.373</b>	<b>0.256</b>	0.389	0.263	0.367	0.283	<b>0.366</b>	<b>0.274</b>	0.384	0.276
	Rain	1.776	<b>1.205</b>	1.776	1.211	1.776	1.208	1.873	3.848	1.883	3.222	<b>1.805</b>	<b>3.046</b>	1.818	1.695	1.818	1.671	<b>1.776</b>	<b>1.208</b>
NOAA	Temperature	0.247	0.242	0.247	0.242	0.247	0.242	0.235	0.231	0.236	0.232	<b>0.231</b>	<b>0.227</b>	0.246	0.242	0.246	0.241	<b>0.245</b>	<b>0.243</b>
	Wind	0.454	<b>0.640</b>	0.454	0.641	<b>0.452</b>	<b>0.640</b>	0.441	0.632	0.441	0.631	<b>0.434</b>	<b>0.623</b>	<b>0.452</b>	0.642	0.453	0.642	<b>0.452</b>	<b>0.640</b>
Average		0.417	<b>0.324</b>	0.417	0.325	<b>0.415</b>	<b>0.324</b>	0.442	0.653	0.437	0.574	<b>0.424</b>	<b>0.551</b>	0.422	0.387	0.422	0.383	<b>0.417</b>	<b>0.325</b>
<i>Cross-domain Generalization</i>																			
FRED	Commodity	<b>0.081</b>	<b>0.044</b>	0.082	0.045	<b>0.081</b>	<b>0.044</b>	0.203	0.061	<b>0.189</b>	<b>0.059</b>	0.197	<b>0.059</b>	0.109	0.047	0.108	0.047	<b>0.107</b>	<b>0.046</b>
	Income	0.296	0.055	0.296	0.055	<b>0.295</b>	<b>0.053</b>	<b>0.319</b>	<b>0.064</b>	0.323	0.088	0.323	0.070	0.301	0.054	0.302	0.054	<b>0.295</b>	<b>0.053</b>
NOAA	Interest rate	0.085	0.075	0.085	<b>0.074</b>	0.085	<b>0.074</b>	0.149	0.058	<b>0.145</b>	<b>0.052</b>	0.146	0.054	0.101	<b>0.077</b>	0.101	0.078	<b>0.100</b>	<b>0.077</b>
	Exchange rate	0.029	0.056	0.029	0.056	0.029	<b>0.055</b>	0.055	0.065	<b>0.053</b>	0.066	0.055	<b>0.063</b>	0.032	0.056	0.032	0.056	<b>0.031</b>	<b>0.055</b>
NOAA	Pressure	0.374	0.260	0.373	0.260	<b>0.372</b>	0.260	0.410	0.313	<b>0.405</b>	0.316	<b>0.405</b>	<b>0.299</b>	0.257	0.356	<b>0.255</b>	0.372	0.263	<b>0.355</b>
	Rain	1.808	0.931	1.808	0.931	<b>1.803</b>	<b>0.783</b>	1.802	2.144	1.802	2.152	<b>1.787</b>	<b>1.831</b>	1.805	1.186	1.805	1.180	<b>1.804</b>	<b>1.178</b>
NOAA	Temperature	0.246	0.243	0.246	0.243	<b>0.245</b>	<b>0.242</b>	0.244	0.248	0.242	0.246	<b>0.240</b>	<b>0.244</b>	0.246	0.243	<b>0.245</b>	0.243	<b>0.245</b>	0.243
	Wind	0.453	0.643	0.453	0.643	<b>0.452</b>	0.643	0.443	0.649	0.442	0.649	<b>0.439</b>	<b>0.646</b>	0.443	0.643	<b>0.645</b>	0.643	<b>0.645</b>	0.643
Average		0.421	0.288	0.422	0.288	<b>0.420</b>	<b>0.269</b>	0.453	0.450	0.450	0.454	<b>0.449</b>	<b>0.408</b>	<b>0.425</b>	0.320	<b>0.425</b>	0.320	0.426	<b>0.319</b>
<i>Out-domain Generalization</i>																			
FRED	Commodity	0.104	0.046	<b>0.103</b>	0.046	<b>0.103</b>	0.046	0.270	<b>0.069</b>	0.265	0.070	<b>0.258</b>	<b>0.069</b>	0.050	<b>0.135</b>	0.050	0.136	<b>0.049</b>	0.140
	Income	0.299	0.056	0.299	0.056	<b>0.298</b>	<b>0.055</b>	0.324	0.063	<b>0.319</b>	<b>0.060</b>	0.335	0.075	0.305	0.056	0.306	0.056	<b>0.304</b>	<b>0.055</b>
NOAA	Interest rate	0.101	0.071	0.101	0.071	<b>0.100</b>	<b>0.070</b>	0.193	0.048	0.191	0.073	<b>0.189</b>	<b>0.046</b>	0.123	0.074	<b>0.120</b>	<b>0.072</b>	<b>0.120</b>	0.073
	Exchange rate	0.034	0.058	0.034	0.058	0.034	0.058	0.077	0.074	<b>0.072</b>									

Table 6: **Performance under conditions of subtle domain shift.** F and N represent the FRED and NOAA datasets, respectively. The number of domains associated with each dataset is denoted accordingly (e.g., F3 represents three source domains from FRED). We systematically conduct experiments by considering all possible combinations for each case and subsequently report the mean performance.

Method	N-HiTS		+ FA (ours)		N-BEATS-I		+ FA (ours)		N-BEATS-G		+ FA (ours)	
	sMAPE	MASE	sMAPE	MASE	sMAPE	MASE	sMAPE	MASE	sMAPE	MASE	sMAPE	MASE
F3	0.023	2.055	0.023	2.055	<b>0.025</b>	<b>2.028</b>	0.027	2.061	0.024	<b>2.064</b>	0.024	2.066
F2N1	0.236	0.244	0.236	<b>0.240</b>	0.210	0.221	<b>0.209</b>	<b>0.220</b>	0.236	<b>0.241</b>	0.236	0.244
F1N2	0.235	0.240	0.235	0.240	0.209	0.220	0.209	<b>0.219</b>	0.235	<b>0.240</b>	<b>0.234</b>	0.241
N3	0.243	0.243	0.243	0.243	<b>0.220</b>	<b>0.224</b>	0.221	0.225	0.242	0.243	<b>0.241</b>	<b>0.242</b>
Average	0.184	0.695	0.184	<b>0.694</b>	0.166	<b>0.673</b>	0.166	0.680	0.184	<b>0.697</b>	0.184	0.698

under such conditions. The results presented in Table 6 demonstrate that our model maintains competitiveness in terms of performance, albeit with some degradation observed in certain cases.

## F Visual Exploration.

### F.1 Qualitative Investigation for Forecasting

We conduct the comparison between baselines (namely, vanilla N-BEATS-G, N-BEATS-I, and N-HiTS) and ours by the visual quality of forecasting. Figure 4 illustrates that the inclusion of feature alignment significantly enhances generalization, enabling baselines to capture finer details in the forecasts. While the forecasting accuracy of the baseline models experiences a substantial degradation in the CDG and ODG scenarios, the accuracy of Feature-aligned N-BEATS demonstrates that the utilization of the feature alignment proves beneficial in mitigating this degradation.

### F.2 Feature Alignment

We perform a comparative analysis of the representations (samples of pushforward measures) obtained from N-BEATS-I and N-HiTS. To visualize the feature measures, we follow the same technique for both with- and without alignment cases, as in Section 5.1. We set UMAP parameters, the number of neighbors, min distance, and metric as 5, 0.1, and Euclidean, respectively. Similar to the findings regarding N-BEATS-G discussed in Section 5.3 of the main paper, two observations are made regarding N-BEATS-I and N-HiTS: (i) Instances are positioned in closer proximity to each other; (ii) The entropy of domains demonstrates a substantial increase. These observations hold true for both N-BEATS-I and N-HiTS. Please refer to Figure 5.

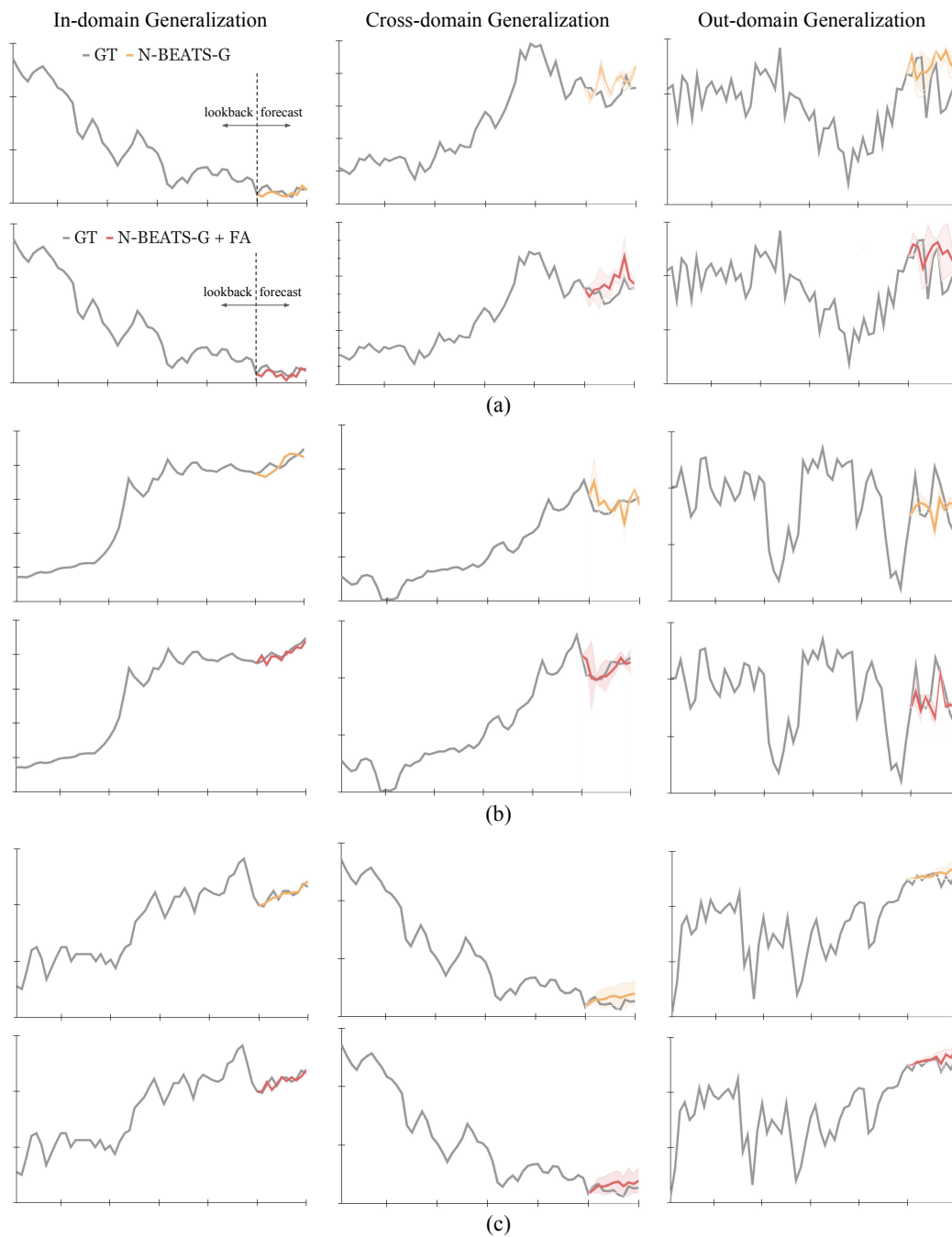


Figure 4: **Visual investigation, our approach with baselines.** (a) Feature-aligned (FA) N-BEATS-G, (b) FA N-BEATS-I, and (c) FA N-HiTS. We calculate the average of all combinations from the source domains, along with their standard deviation. Note that there is one case for IDG.

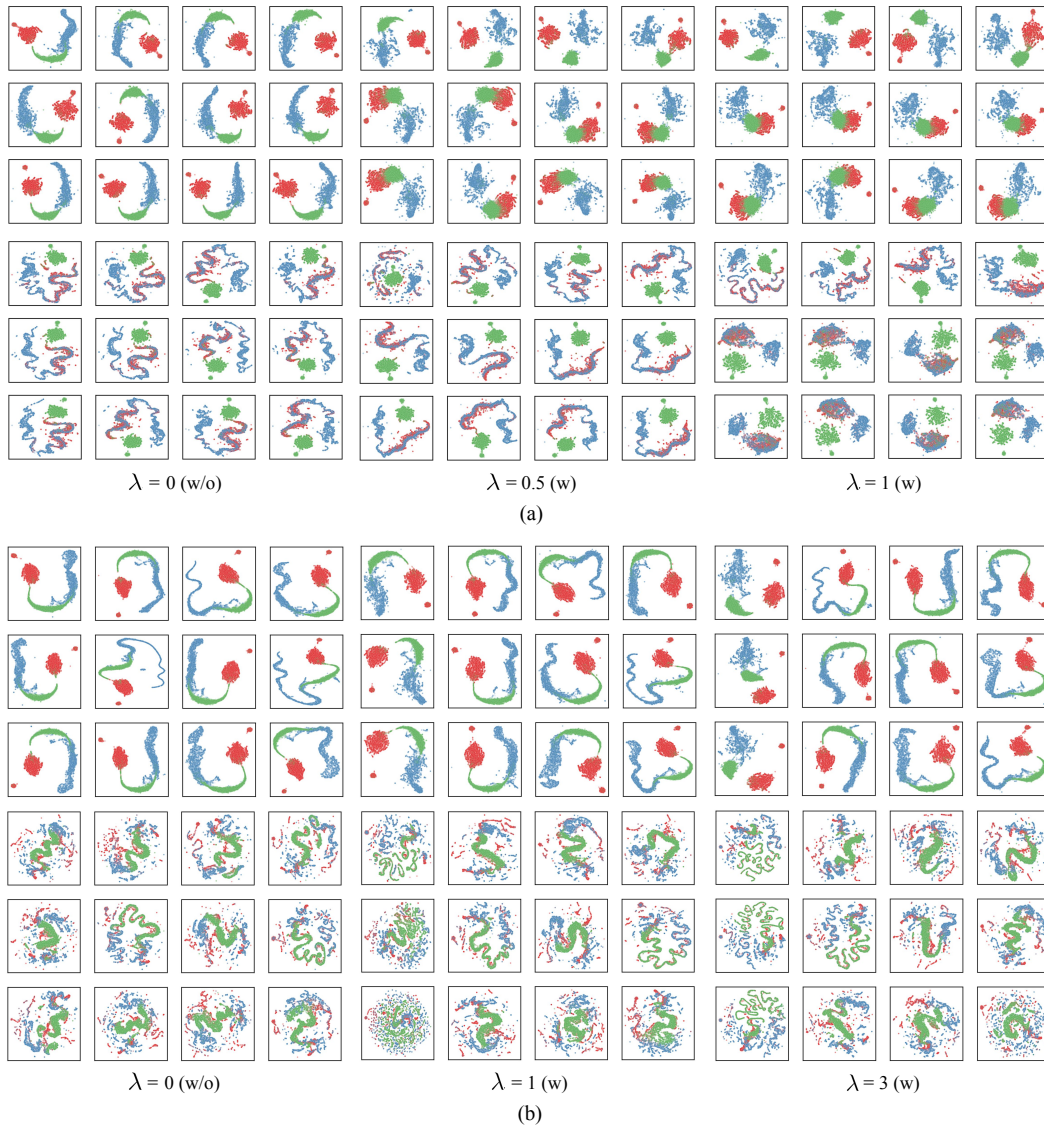


Figure 5: **Visual comparison between with alignment (w) and without alignment (w/o).** (a) N-BEATS-I and (b) N-HiTS. In both sets (a) and (b), each first case illustrates a convergence among the instances, resulting in increased proximity. Conversely, the subsequent cases depict a clear manifestation of heightened entropy.